
01 Jan 2023

3D CFD Simulation of a Bubble Column with Internals: Validation of Interfacial Forces and Internal Effects for Local Gas Holdup Predictions

Hayder Al-Naseri


Joshua P. Schlegel

Missouri University of Science and Technology, schlegelj@mst.edu

Muthanna H. Al-Dahhan

Missouri University of Science and Technology, aldahhanm@mst.edu

Follow this and additional works at: https://scholarsmine.mst.edu/nuclear_facwork

 Part of the [Biochemical and Biomolecular Engineering Commons](#), and the [Nuclear Engineering Commons](#)

Recommended Citation

H. Al-Naseri et al., "3D CFD Simulation of a Bubble Column with Internals: Validation of Interfacial Forces and Internal Effects for Local Gas Holdup Predictions," *Industrial and Engineering Chemistry Research*, American Chemical Society, Jan 2023.

The definitive version is available at <https://doi.org/10.1021/acs.iecr.3c01404>

This Article - Journal is brought to you for free and open access by Scholars' Mine. It has been accepted for inclusion in Nuclear Engineering and Radiation Science Faculty Research & Creative Works by an authorized administrator of Scholars' Mine. This work is protected by U. S. Copyright Law. Unauthorized use including reproduction for redistribution requires the permission of the copyright holder. For more information, please contact scholarsmine@mst.edu.

3D CFD Simulation of a Bubble Column with Internals: Validation of Interfacial Forces and Internal Effects for Local Gas Holdup Predictions

Hayder Al-Naseri, J. P. Schlegel, and Muthanna H. Al-Dahhan*



Cite This: *Ind. Eng. Chem. Res.* 2023, 62, 14679–14699

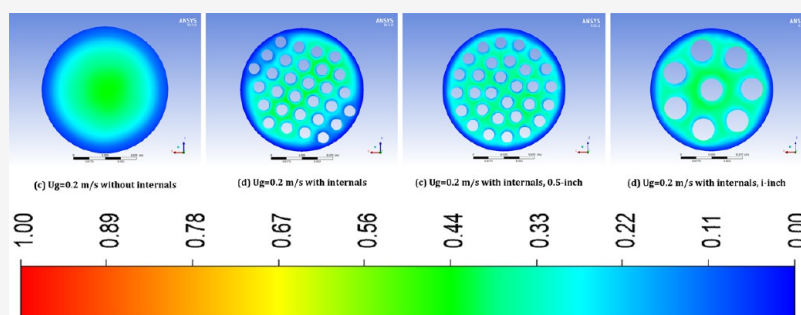


Read Online

ACCESS |

Metrics & More

Article Recommendations



ABSTRACT: CFD models (turbulent models and interfacial forces) incorporated with the population balance model (PBM) have been validated, azimuthally, with the gamma-ray-computed tomography (CT) results to address the effect of the presence of internals with different arrangements and diameters. The superficial gas velocity applied was varied from 0.05 to 0.45 m/s. The results exhibit the capability to predict the hydrodynamics of the bubble column, further incorporating the population balance model and promoting the prediction of simulation in high superficial gas velocity. The effect of internals revealed that the gas holdup was significantly enhanced in the bubble column's wall region, while the gas holdup was increased remarkably in the center and the wall regions of the bubble column equipped by internals of 1 in. diameter more than in internals of 0.5 in. However, internals with a hexagonal arrangement increase the gas holdup in the central region and less in the wall than in the circular arrangement.

1. INTRODUCTION

Bubble column reactors with and without internals have been utilized widely in different fields such as chemical, petrochemical, wastewater treatment, bioprocess, and metallurgical industries because of their high mass and heat transfer coefficients, good mixing and thermal control, low cost, no movable parts, and high conversion.^{1–5} The intensity of internal tubes for heat exchanging varies from low intensity (methanol synthesis of 5% coverage of cross-sectional area) to high intensity (Fischer–Tropsch synthesis of about 25% coverage of cross-sectional area) based on the heat of reaction of the system for either exothermic or endothermic. In spite of the competitive features, the disadvantages of bubble column reactors are difficult to design due to the interaction between the phases, back-mixing, and the liquid circulation.^{6–10} Hence, numerous studies to investigate the effects of the physical properties of gas and liquid phases, the presence of internals, column dimensions, and the sparger design have been conducted either experimentally^{2,5,9,11–15} or theoretically^{10,16–24} to improve the column reactor performance, design, and scale-up. Furthermore, the experimental work has provided valuable benchmark data to

validate computational fluid dynamics (CFD) models and simulation.

Recently, CFD simulations have been used widely in industry and research to investigate the hydrodynamics of bubble columns to improve the operation analysis, design, and scale-up. Therefore, CFD simulation substituted full-scale experiments in the bubble column, which are expensive. Hence, validating CFD models is essential for studying bubble columns and gas–liquid systems to consider a more cost-effective approach.²⁵

Two approaches of Eulerian–Lagrangian,^{26–28} and Eulerian–Eulerian^{29–33} approaches have been employed for the CFD simulations of bubble columns or gas–liquid flow systems. In the Eulerian–Lagrangian model, the continuous phase is described by a Eulerian representation. In contrast, the dispersed

Received: April 27, 2023

Revised: August 16, 2023

Accepted: August 18, 2023

Published: August 30, 2023



phase is treated as discrete bubbles. Each bubble is tracked by solving the equations of motion for individual bubbles, which requires tracking the dynamics of each bubble. Therefore, it is usually applied to cases with low superficial gas velocity due to computer limitations. The Eulerian–Eulerian model treats dispersed (gas bubbles) and continuous (liquid) phases as an interpenetrating continuum and describes the motion of gas and liquid phases in an Eulerian frame of reference. The Eulerian–Eulerian method is often used for gas–liquid bubble column systems because memory storage requirements and computer power demand depend only on the number of computational cells considered instead of the number of bubbles. Therefore, the Eulerian–Eulerian approach has been used to simulate the hydrodynamics of bubble columns in a wide range of superficial gas velocities and large scales.³² However, another approach of the volume of fluid (VOF) solves the instantaneous Navier–Stokes equations to obtain the gas and liquid flow fields with an extremely high spatial resolution. The evaluation of the gas–liquid interface is tracked using a volume-tracking scheme. Thus, the VOF method is limited to a small number of bubbles, less than 10 bubbles in the flow field. Therefore, this approach has not been implemented on the full scale of a bubble column.

Accordingly, in this work, the Eulerian–Eulerian approach has been used to simulate bubble columns with and without internals. While many studies reported in the literature on developing and implementing CFD on bubble columns without internals have been reported, very limited studies on the effect of internals on the hydrodynamics of bubble columns have been reported using CFD. Moreover, these reported CFD simulations for bubble columns with internals have not been validated due to the lack of experimental data in bubble columns with intense internals. The following is a summary of these studies.

Larachi et al.³⁴ simulated, for the first time, the impacts of liquid circulation in the bubble column in the presence of internals using two-fluid Euler approach continuum transient three-dimensional (3D) simulations. Bubble columns with five internal configurations, which covers 2 and 16.2% of the cross-sectional area of the bubble and without internals, were simulated and performed at a superficial gas velocity of $U_g = 0.12$ m/s. The simulation results of the bubble column without internals were validated with the experimental results reported by Sanyal et al.³¹ using the radioactive particle tracking (RPT) for liquid velocity measurements and computerized gamma-ray tomography (CT) for gas holdup measurements. However, the CFD results with internals were not validated due to a lack of experimental data at the time of this study. Such results revealed that the presence of internals has noticeable impacts on column hydrodynamics. Subsequently, Guo and Chen³⁵ have investigated the impacts of vertical internals with circular configuration on the hydrodynamics of the bubble column. They used the Eulerian two-fluid model coupled with a population balance model (TFM-PBM) and applied interfacial forces, including drag force, lift force, and wall lubrication force. Results of the local gas holdup were validated with the benchmark experimental data of Kagumba and Al-Dahhan.³⁶ They investigated the effects of internals with different sizes and two configurations (hexagonal and circular) of internals on the bubble dynamics using an advanced four-point optical fiber probe. However, the numerical data revealed that the radial wall lubrication force greatly affects the radial distribution of the time-averaged gas holdup, especially in the internals affecting regions. When the internals were present, the turbulent dissipation rates increased significantly in the gaps between

the internal walls and more bubbles with smaller bubble sizes were predicted in the bubble column. Meanwhile, the gas holdup increased with dense internal insertion, especially in r/R equal to 0.6–0.9 region. The internals and the configurations influence the overall liquid circulation.

Guan and Yang³⁷ studied the influence of the interfacial forces, including drag force, lift force, turbulent dispersion force, and wall force on the hydrodynamics in pilot-scale bubble columns with internals, which covers 5% of the cross-sectional area of the bubble column with a hexagonal configuration. The numerical results of the local gas holdup and the axial liquid velocity were validated against the experimental data reported by Yu et al.³⁸ The CFD results revealed that the lift force, turbulent dispersion force, and wall force are optional interfacial forces in the simulation of the bubble column without internals. In contrast, in the simulation case of the bubble column with internals, the interfacial forces are significant to properly predict flow characteristics. Furthermore, despite the insignificant effect on gas holdup, the presence of internals enhances large-scale liquid circulation due to the remarkable decrease in turbulent viscosity. Bhusare et al.²¹ performed a numerical simulation for bubble columns with and without internals by using the OpenFOAM CFD tool to study the capability of the OpenFOAM CFD tool to simulate the bubble column and to address the effect of the presence of internals on the hydrodynamics of the bubble column. The OpenFOAM CFD tool results have been validated locally with the experimental results of gas holdup and axial liquid velocity. However, the obtained results show that the OpenFOAM simulations agree with the experimental data. In addition, it is observed that the overall flow pattern in the column remains unaffected by the internals, which covers 9–23% of the column's cross-sectional area. With increasing the number of internals, the averaged gas holdup was increased and the axial liquid velocity was decreased, which is attributed to reducing the fluctuations in the column with internals compared to that of the column without internals.

Recently, Agahzamin and Pakzad³⁹ investigated the effects of internals, covering 21.5% of the total cross-sectional area of the bubble column, on the hydrodynamics of the bubble column by utilizing the Eulerian–Eulerian model incorporated with population balance model (PBM) and interfacial forces including the lift force and wall force. Validating the interfacial forces and the simulation code was executed by comparing the local gas holdup of the numerical results with the experimental data of Youssef.⁴⁰ The results reported that the simulation model would agree with the experimental data by choosing the appropriate interfacial forces.

Accordingly, in this study, the interfacial forces that embedded the drag, lift, wall lubrication, and turbulent dispersion (using different models) have been evaluated to simulate the bubble column with internals and without internals (25% of cross-sectional area covering) using CFD with the Eulerian–Eulerian approach. The CFD simulations have been validated with the experimental data reported by Al Mesfer et al.⁴¹ and Sultan et al.³⁴ that were conducted in a bubble column with and without internals by using the gamma-ray computed tomography (CT) technique. Meanwhile, the renormalization group RNG ($k - \epsilon$) turbulence model has been used. The effects of internals using different configurations and diameters of the tube on the gas holdup profiles have been simulated by using the 3D CFD simulation. The Eulerian–Eulerian approach coupled with population bubble model (PBM) has been utilized. Therefore, this work has been accomplished through three

steps: (1) investigating the sensitivity of the numerical solution regarding the grid size effect, the time-collection effect, and the time steady-state effect; (2) validation of the interfacial forces and the turbulence models; and (3) investigating the effects of the presence of internals, the configurations of internals, and the size of the internal rod on the local gas holdup. The 3D CFD simulation has been performed on the same experimental setup used by Al Mesfer et al.⁴¹ and Sultan et al.^{3,4} with the Eulerian–Eulerian approach coupled with the population balance model (PBM).

1.1. Governing Equations of the Eulerian–Eulerian Approach. As mentioned earlier, in this work, the Eulerian–Eulerian approach was used for the 3D CFD simulations. The Eulerian modeling framework is based on ensemble-averaged mass and momentum transport equations governing each phase.⁴² The continuous phase in the approach is the liquid phase ($q = L$) and the gas phase (bubble) as the disperse phase ($q = G$).

The continuity equation for a flow with equally sized bubbles of diameter d_b , without mass transfer between the phases, can be written as shown in eq 1

$$\frac{\partial(\rho_q \alpha_q)}{\partial t} + \nabla \cdot (\rho_q \alpha_q \mathbf{u}_q) = 0 \quad (1)$$

The momentum equation for the momentum conservation in the control volume of multiphase flows is described by Navier–Stokes as shown in eq 2

$$\begin{aligned} \frac{\partial}{\partial t}(\alpha_q \rho_q \mathbf{u}_q) + \nabla \cdot (\alpha_q \rho_q \mathbf{u}_q \mathbf{u}_q) \\ = \underbrace{-\alpha_q \nabla p}_{\text{I}} + \underbrace{\nabla \cdot (\alpha_q \boldsymbol{\tau}_q)}_{\text{II}} + \underbrace{\alpha_q \rho_q \vec{g}}_{\text{III}} + \underbrace{F_q}_{\text{IV}} \end{aligned} \quad (2)$$

The terms I, II, III, and IV on the right-hand side of eq 2 are the pressure gradient (∇p), the stress tensor ($\boldsymbol{\tau}_q$), the gravitational force (\vec{g}), and the interfacial forces (F_{pq}), respectively, which describe all forces that are acting on the phase in the control q volume. The stress tensor $\boldsymbol{\tau}_q$ for the q phase is shown in eq 3 (term II of eq 2), where μ_{eff} is the effective viscosity. However, $\mu_{\text{eff,L}}$ is the effective viscosity for the liquid phase, which is a result of three contributions as given in eq 4: $\mu_{L,L}$, $\mu_{T,L}$, and $\mu_{B,L}$ represent the molecular viscosity, the shear-induced turbulence viscosity, and the bubble-induced turbulence viscosity, respectively. Sato et al.⁴³ proposed an exertion for the viscosity due to the turbulence induced by the movement of the bubbles as shown in eq 5, where the $C_{\mu,B}$ is a constant model equal to 0.6 as reported in previous studies.^{44,45} The effective gas viscosity $\mu_{\text{eff,G}}$ depends on the effective liquid viscosity and can be expressed as given in eq 6

$$\boldsymbol{\tau}_q = \mu_{\text{eff},q} \left(\nabla \mathbf{u}_q + (\nabla \mathbf{u}_q)^T - \frac{2}{3} I (\nabla \cdot \mathbf{u}_q) \right) \quad (3)$$

$$\mu_{\text{eff,L}} = \mu_{L,L} + \mu_{T,L} + \mu_{B,L} \quad (4)$$

$$\mu_{B,L} = \rho_L C_{\mu,B} \alpha_G d_B |\mathbf{u}_G - \mathbf{u}_L| \quad (5)$$

$$\mu_{\text{eff,G}} = \frac{\rho_G}{\rho_L} \mu_{\text{eff,L}} \quad (6)$$

1.2. Turbulence Closure Models. Although the two-equation models like the $k - \varepsilon$ model suffer from the assumption of isotropic eddy viscosity, they still score over the high-fidelity

models like the Reynolds stress model, as they are simple and less computationally demanding. For gas–liquid systems, the mixture $k - \varepsilon$ model^{46,47} proves to be more reliable for a wide range of dispersed phase fractions when compared to earlier works that considered only the turbulent kinetic energy in the continuous phase. As $k - \varepsilon$ is employed for turbulence modeling, the turbulent eddy viscosity is calculated using the $k - \varepsilon$ turbulence model, where k represents the turbulent kinetic energy and ε is its dissipation rate in the liquid phase. k and ε determine the energy in turbulence and the scale of the turbulence, respectively. The turbulent eddy viscosity, $\mu_{T,L}$, the turbulent kinetic energy, k , and the energy dissipation rate, ε , can be expressed by the following equations⁴⁸

$$\mu_{T,L} = C_{\mu} \rho_L \frac{k^2}{\varepsilon} \quad (7)$$

$$\begin{aligned} \frac{\partial(\alpha_L \rho_L k_L)}{\partial t} + \nabla \cdot (\alpha_L \rho_L k_L \mathbf{u}_L) \\ = \nabla \cdot \left(\alpha_L \frac{\mu_{T,L}}{\sigma_k} \nabla k_L \right) + \alpha_L (G_{k,L} - \rho_L \varepsilon_L) + S_k \end{aligned} \quad (8)$$

$$\begin{aligned} \frac{\partial(\alpha_L \rho_L \varepsilon_L)}{\partial t} + \nabla \cdot (\alpha_L \rho_L \varepsilon_L \mathbf{u}_L) \\ = \nabla \cdot \left(\alpha_L \frac{\mu_{T,L}}{\sigma_\varepsilon} \nabla \varepsilon_L \right) + \alpha_L \frac{\varepsilon_L}{k_L} (C_{\varepsilon 1} G_{k,L} - C_{\varepsilon 2} \rho_L \varepsilon_L) + S_\varepsilon \end{aligned} \quad (9)$$

The standard model constants are $C_{\varepsilon 1} = 1.44$, $C_{\varepsilon 2} = 1.92$, $C_{\mu} = 0.09$, $\sigma_k = 1$, and $\sigma_\varepsilon = 1.3$. The term G in eqs 8 and 9 is the production of the turbulent kinetic energy, which is described by

$$G_{k,L} = \mu_{t,L} (\nabla \bar{v}_L + (\nabla \bar{v}_L)^T) : \nabla \bar{v}_L \quad (10)$$

1.3. Interfacial Forces (Momentum Transfer). Interfacial forces, the momentum transfer between the dispersion phase (bubbles) and the continuous phase (liquid), are essential to modeling the gas–liquid flows due to significantly administrating the distribution of gas and liquid phases in the flow volume. The fourth term (F_{pq}) on the right-hand side (RSH) of the momentum eq 2 represents the interfacial forces that include the drag force (F_{drag}), lift force (F_{lift}), wall lubrication force ($F_{\text{wall lub.}}$), turbulent dispersion force ($F_{\text{turbulent dis.}}$), and virtual force (F_{virtual}) as shown in eq 11⁴⁹

$$F_q = F_{\text{drag}} + F_{\text{lift}} + F_{\text{turbulent dis.}} + F_{\text{wall lub.}} + F_{\text{virtual}} \quad (11)$$

1.3.1. Drag Models. The drag force is the resistance experienced by a bubble moving within the continuous phase due to the shear stress and the pressure distribution around the moving bubble surface; thus, it is the main reason to deform the bubble shape.^{49,50} Hence, eq 12 has been formulated to calculate the drag force, where C_D is the drag coefficient that is a function of the bubble's Reynolds number $C_D(Re_B)$, known as the drag curve, which can be correlated for individual bubbles for different flow regions based on the Re_B as given in eq 13

$$F_{\text{drag}} = \frac{3}{4} \alpha_G \rho_L \frac{C_D}{d_B} (\mathbf{u}_G - \mathbf{u}_L) |\mathbf{u}_G - \mathbf{u}_L| \quad (12)$$

$$Re_B = \frac{\rho_L d_B (\mathbf{u}_G - \mathbf{u}_L)}{\mu_L} \quad (13)$$

In this work, different modeling formulations to calculate the drag coefficient (C_D) have been applied like Grace et al.,⁵¹ Tomiyama,⁵² Morsi and Alexander,⁵³ and Schiller and Naumann.⁵⁴ These are discussed below.

1.3.1.1. Grace et al.⁵¹ Model. The Grace et al.⁵¹ model classified the calculation of the drag coefficient based on the shape of a bubble that is related to the flow regime. Therefore, the Grace et al.⁵¹ model properly represents the gas–liquid system flow through three drag coefficients $C_{D_{\text{sphere}}}$, $C_{D_{\text{cap}}}$, and $C_{D_{\text{ellipse}}}$, which represent the bubbly, transition, and churn turbulent flow regimes, respectively

$$C_D = \max(\min(C_{D_{\text{ellipse}}}, C_{D_{\text{cap}}}), C_{D_{\text{sphere}}}) \quad (14)$$

$$C_{D_{\text{sphere}}} = \begin{cases} 24/Re_B & Re_B < 0.01 \\ 24(1 + 0.15Re_B^{0.687}) & Re_B \geq 0.01 \end{cases} \quad (15)$$

$$C_{\text{cap}} = \frac{8}{3} \quad (16)$$

$$C_{\text{ellipse}} = \frac{4}{3} \frac{gd_B(\rho_L - \rho_G)}{U_t^2 \rho_L} \quad (17)$$

U_t is the terminal velocity of the bubble that was correlated as in eq 18

$$U_t = \frac{\mu_L}{\rho_L d_B} M_o^{-0.149} (J - 0.857) \quad (18)$$

M_o is the Morton number given by eq 19, and J is given by the piecewise function as in eq 20

$$M_o = \frac{\mu_L^4 g(\rho_L - \rho_G)}{\rho_L^2 \sigma^3} \quad (19)$$

$$J = \begin{cases} 0.94H^{0.757} & 2 < H \leq 59.3 \\ 3.42H^{0.441} & H \geq 59.3 \end{cases} \quad (20)$$

$$H = \frac{3}{4} E_o M_o^{-0.149} \left(\frac{\mu_L}{\mu_{\text{ref}}} \right)^{-0.14} \quad (21)$$

E_o is the Eötvös number, which is expressed as follows

$$E_o = \frac{g(\rho_L - \rho_G)d_B^2}{\sigma}$$

1.3.1.2. Tomiyama⁵² Model. Tomiyama⁵² developed a drag coefficient model, which considers the fluid properties, as given in eq 23, and hence, the degree of contamination of the continuing phase was taken into account

$$C_D = \max\left(\min\left(\frac{24}{Re}(1 + 0.15Re^{0.687}), \frac{72}{Re}\right), \frac{8}{3} \frac{E_o}{E_o + 4}\right) \quad (22)$$

1.3.1.3. Morsi–Alexander⁵³ Model. The Morsi and Alexander⁵³ model calculates the drag coefficient C_D by the given eq 23, while Re_B is the bubble's Reynolds number as defined by eq 13 and the constants a_i are coefficients that are calculated based on the Reynolds number, with more details being found in Fluent⁴⁸

$$C_D = a_1 + \frac{a_2}{Re_B} + \frac{a_3}{Re_B^2} \quad (23)$$

1.3.1.4. Schiller and Naumann⁵⁴ Model. The Schiller and Naumann⁵⁴ model is given in eq 24

$$C_D = \begin{cases} 24(0.15Re_B^{0.687})/Re_B & Re_B \leq 1000 \\ 0.44 & Re_B \geq 1000 \end{cases} \quad (24)$$

1.3.2. Lift Models. The lift force is a lateral force that a bubble experiences and is perpendicular to the direction of the bubble's motion due to the horizontal velocity gradient; thereby, the lift force has been correlated with the local liquid velocity and the slip velocity as shown in eq 25

$$F_{\text{lift}} = C_{\text{L}} \rho_L \alpha_G (\mathbf{u}_L - \mathbf{u}_G) \times (\nabla \times \mathbf{u}_L) \quad (25)$$

According to Bothe et al.⁵⁵ and Lucas et al.,⁵⁶ they suggested that the lift force is sensitive to the bubble size. Therefore, the small bubble size is driven by positive lift forces, whereas the large bubble size is driven by a negative lift force in the opposite direction, and hence, it migrates toward the center region of the bubble column. Meanwhile, Tomiyama⁵² quantified and classified the small bubble size and large bubble size by $d_B \leq 5.8$ mm and $d_B \geq 5.8$ mm, respectively. Therefore, the lift force significantly affects the radial profiles of the gas holdup and, hence, the liquid velocity.

1.3.3. Wall Lubrication Models. The wall lubrication force is a force that is responsible for pushing the bubbles away from the vicinity of the wall area and generated as a result of the surface tension of bubbles, which in turn reduce the gas holdup in the wall area.⁵⁷ However, the general model for the wall lubrication force is given in eq 26

$$F_{\text{wall lub}} = C_{\text{W}} \rho_L \alpha_G |(\mathbf{u}_L - \mathbf{u}_G)_{\parallel}|^2 \vec{n}_W \quad (26)$$

where $|(\mathbf{u}_L - \mathbf{u}_G)_{\parallel}|$ is the phase relative velocity component tangential to the wall surface, and \vec{n}_W is the unit normal pointing away from the wall. There are different models to assess the wall lubrication coefficient C_W .

1.3.3.1. Antal et al.⁵⁸ Model. Antal et al.⁵⁸ proposed a model given in eq 27 to compute the wall lubrication coefficient C_W

$$C_W = \max\left(0, \frac{C_{W1}}{d_B} + \frac{C_{W2}}{y_W}\right) \quad (27)$$

where $C_{W1} = -0.01$ and $C_{W1} = 0.05$ are the nondimensional coefficient, d_B is the bubble diameter, and y_W is the distance to the nearest wall. Noting, C_W has a nonzero value only within a thin layer adjacent to the wall that satisfies $y_W \leq -(C_{W2}/C_{W1})d_B$.

1.3.3.2. Tomiyama⁵² Model. Tomiyama⁵² has modified the wall lubrication coefficient formulated by Antal et al.⁵⁸ based on the data obtained from experiments with the flow of air bubbles in glycerin in a pipe. Tomiyama model, as given in eq 28, considers the bubble column diameter and the fluid properties. Although this model is superior to Antal's model, it is restricted to the flow in column geometries because of the dependence on the column diameter D ⁵⁹

$$C_W = C_o \frac{d_B}{2} \left(\frac{1}{y_W^2} - \frac{1}{(D - y_W)^2} \right) \quad (28)$$

where D is the column diameter, and C_o is a coefficient that depends on the Eötvös number E_o as given in eq 29

$$C_o = \begin{cases} 0.47 & E_o < 1 \\ e^{10.933E_o + 0.179} & 1 \leq E_o \leq 5 \\ 0.00599E_o - 0.0187 & 5 < E_o \leq 33 \\ 0.17933 & 33 \leq E_o \end{cases} \quad (29)$$

1.3.3.3. *Frank et al.*⁵⁹ *Model*. Frank et al.⁵⁹ proposed a model that calculates the wall lubrication coefficient independently of the column diameter, as given in eq 30, in contrast to the Tomiyama⁵² model

$$C_w = C_o \max\left(0, \frac{1}{C_{wd}} \times \frac{1 - y_w/C_{wc}d_B}{y_w(y_w/C_{wc}d_B)^{m-1}}\right) \quad (30)$$

where C_o is determined as in eq 29, C_{wd} is the damping coefficient, by default $C_{wd} = 6.8$, which determines the relative magnitude of the force, m is the constant of the power law, $m = 1.5$ and 2 , and C_{wc} is the cutoff coefficient that determines the distance to the wall within which the force is active.⁴⁸

1.3.4. *Turbulent Dispersion Models*. Turbulent dispersion force is a turbulent interphase transfer, which induces turbulent diffusion in the dispersed phase (the gas phase in this study). Hence, it is taken as a function of the turbulent kinetic energy in the continuous phase (the liquid phase in this study).^{49,57} The general formula is given in eq 31

$$F_{T,L} = -F_{T,G} = -f_{T,limiting} K_{GL} \mathbf{u}_{dr} \quad (31)$$

where $F_{T,L}$ and $F_{T,G}$ are the turbulent dispersion of the liquid phase and the gas phase, respectively, $f_{T,limiting}$ is a factor that can be used to impose a limiting function on the turbulent dispersion force, K_{GL} is the exchange coefficient ($K_{GL} = \rho_G f d_B a_G / 6 \tau_G$), and \mathbf{u}_{dr} is the drift velocity that accounts for the dispersion of the gas phase due to transport by turbulent fluid motion.

1.3.4.1. *Simonin*⁶⁰ *Model*. Simonin and Viollet⁶⁰ formulated a new model to calculate the turbulent dispersion force as given in eq 32

$$F_{T,L} = -F_{T,G} = C_{TD} K_{GL} \frac{D_{TGL}}{\sigma_{GL}} \left(\frac{\nabla \alpha_G}{\alpha_G} - \frac{\nabla \alpha_L}{\alpha_L} \right) \quad (32)$$

where C_{TD} and σ_{GL} are the user-modifiable constants that are set to 1 and 0.75 by default, respectively, and D_{TGL} is the fluid-particulate dispersion tensor.

1.3.4.2. *Burns et al.*⁶¹ *Model*. Burns et al.⁶¹ derived a model based on the Favre averaging of the drag term. The final expression is similar to that of Simonin's model. For the Burns et al.⁶¹ model, the dispersion scalar is estimated by the turbulent viscosity of the continuous phase as shown in eq 33

$$\mathbf{D}_L = \mathbf{D}_G = \mathbf{D}_{TGL} = \mu_{TL} / \mu_{TG} \quad (33)$$

and

$$F_{T,L} = -F_{T,G} = C_{TD} K_{GL} \frac{D_{TGL}}{\sigma_{GL}} \left(\frac{\nabla \alpha_G}{\alpha_G} - \frac{\nabla \alpha_L}{\alpha_L} \right) \quad (34)$$

Here, $C_{TD} = 1$ and $\sigma_{GL} = 0.9$ by default.

1.4. **Population Balance Model (PBM)**. According to what was mentioned, the interfacial forces and the turbulent model depend on the bubble diameter. Hence, an assumption that the bubbles have one diameter, in turn, significantly influences the simulation results of the momentum transfer between two phases, particularly the simulation in the transition and the

churn turbulent flow regimes, where the bubbles exist in a wide spectrum of bubble sizes.^{6,36,62} Therefore, since bubble breakup and coalescence exist in bubble columns within the transition and churn turbulent heterogeneous flow regimes, the range of bubble diameter should be considered in the simulation. The usual approach is to use population balance models that describe the variation in a given population property over space and time in a velocity field. In bubble column modeling, population balance models are applied to determine the bubble size distribution over space and time and how this distribution develops due to the breakup and coalescence processes. The general form of the PBM equation for the gas–liquid can be expressed in eq 35

$$\frac{\partial n(v, t)}{\partial t} + \frac{\nabla \cdot [U_b n(v, t)]}{I} = \frac{S_i}{III} \quad (35)$$

where the bracketed terms represent time variation (I) and convection (II), while term (III) is the net source or sink term of the i -th bubble group generated by bubble coalescence and breakup as expressed in eq 36

$$S_B = B_{c,i} - D_{c,i} + B_{b,i} - D_{b,i} \quad (36)$$

Here, $B_{c,i}$, $D_{c,i}$, $B_{b,i}$, and $D_{b,i}$ are the source terms of birth due to coalescence, death due to coalescence, birth due to breakage, and death due to breakage, respectively. The population balance equation (PBE) can be solved by different methods, such as the discrete method, the standard method of moments (SMMs), the quadrature method of moments (QMOMs), etc. It is based on the continuous particle size distribution with a set of discrete size classes, and a pivot size represents each class x_i , showing the outstanding characteristics of robust numeric and directly giving the particle size distribution (PSD). Equation 35 is integrated over each size interval $[v_i, v_{i+1}]$, resulting in eq 37

$$\begin{aligned} \frac{\partial N_i(t)}{\partial t} + \nabla \cdot [U_b N_i(t)] \\ = \frac{1}{2} \int_{v_i}^{v_{i+1}} dv \int_0^v n(v - \hat{v}, t) n(\hat{v}, t) a(v - \hat{v}, \hat{v}) d\hat{v} \\ - \int_{v_i}^{v_{i+1}} n(v, t) dv \int_0^\infty n(\hat{v}, t) a(v, \hat{v}) d\hat{v} \\ + \int_{v_i}^{v_{i+1}} dv \int_0^\infty \beta(v, \hat{v}) b(\hat{v}) n(\hat{v}, t) d\hat{v} \\ - \int_{v_i}^{v_{i+1}} b(v) n(v, t) dv \end{aligned} \quad (37)$$

The population in a representative volume x_i has a fraction of bubbles born in the size range (x_i, x_{i+1}) or (x_{i-1}, x_i) . For bubbles born in the size range (x_i, x_{i+1}) , bubbles with a percentage of $\lambda_1(v, x_i)$ are assigned to x_i , and for those born in the range (x_{i-1}, x_i) , bubbles with a percentage of $\lambda_2(v, x_{i+1})$ are assigned to x_{i+1} . The values of $\lambda_1(v, x_i)$ and $\lambda_2(v, x_i)$ are given by the following equations

$$\lambda_1(v, x_i) x_i + \lambda_2(v, x_{i+1}) x_{i+1} = v \quad (38)$$

$$\lambda_1(v, x_i) + \lambda_2(v, x_{i+1}) = 1 \quad (39)$$

After all terms in eq 37 are reconstructed, the final discrete PBM is expressed in eq 40

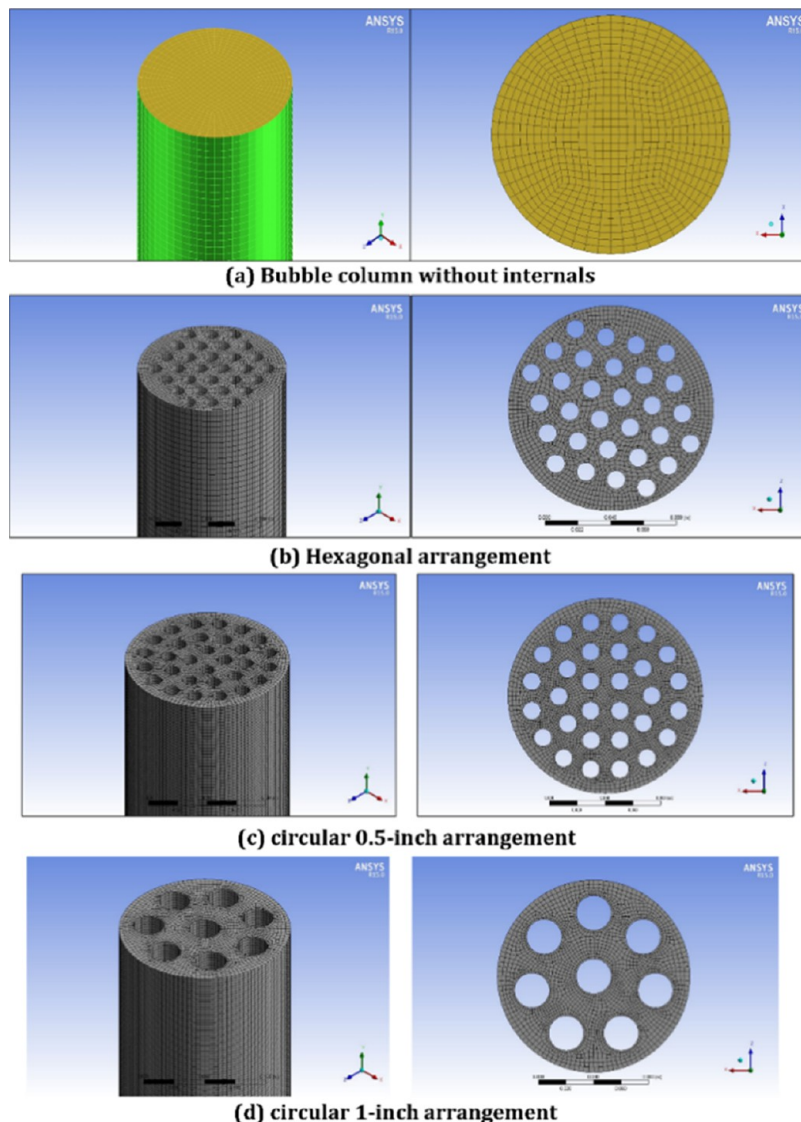


Figure 1. Grid used in CFD simulations: (a) bubble column without internals, (b) bubble column with internals of hexagonal arrangement, (c) bubble column with internals of circular 0.5 in. arrangement, and (d) bubble column with internals of circular 1 in. arrangement.

$$\begin{aligned} & \frac{\partial N_i(t)}{\partial t} + \nabla \cdot [U_b N_i(t)] \\ &= \sum_{g_{i-1} \leq (g_j + g_k) \leq g_{i+1}}^{j \geq k} \left(1 - \frac{1}{2} \delta_{j,k} \right) \omega_{i,jk} N_j(t) N_k(t) - N_i(t) \\ & \quad \sum_{k=1}^M a_{j,k} N_k(t) + \sum_{k=i}^M \psi_{i,k} b(g_k) N_k(t) - b(g_i) N_i(t) \end{aligned} \quad (40)$$

$$\omega_{i,jk} = \begin{cases} (x_{i+1} - v) / (x_{i+1} - x_i), & x_i < v \leq x_{i+1} \\ (v - x_{i-1}) / (x_i - x_{i-1}), & x_{i-1} < v \leq x_i \end{cases} \quad (41)$$

$$\begin{aligned} \psi_{i,k} &= \int_{x_i}^{x_{i+1}} \frac{x_{i+1} - v}{x_{i+1} - x_i} \beta(v, x_k) dv \\ & \quad + \int_{x_{i-1}}^{x_i} \frac{v - x_{i-1}}{x_i - x_{i-1}} \beta(v, x_k) dv \end{aligned} \quad (42)$$

Here, the breakup rate $b(v)$ proposed by Luo and Svendsen⁶³ and the aggregation rate $a_{i,j}$ of Luo⁶⁴ are used. The formulas are described briefly as follows

$$\begin{aligned} b(v) &= 0.9238(1 - \alpha_g)^n \left(\frac{\epsilon}{d^2} \right)^{1/3} \\ & \quad \int_{\xi_{\min}}^1 \frac{(1 + \xi)^2}{\xi^{11/3}} \exp\{-12[f^{2/3} + (1 - f)^{1/3} - 1]\sigma \\ & \quad \rho^{-1} \epsilon^{-2/3} d^{-5/3} \xi^{-11/3}\} d\xi \end{aligned} \quad (43)$$

$$\begin{aligned} a_{i,j} &= \frac{1.43\pi}{4} (d_i^2 + d_j^2) (d_i^{3/2} + d_j^{3/2})^{1/2} \epsilon \\ & \quad \exp(-t_{\text{drainage}}/t_{\text{contact}}) \end{aligned} \quad (44)$$

f is the volume fraction of one daughter bubble, and ξ is the ratio of the eddy size to the parent bubble. The bubbles with different sizes are classified into 10 groups for the churn turbulent flow regime simulation and four groups for the bubbly flow regime.

2. NUMERICAL DETAILS

The numerical solutions have been accomplished using commercial computational fluid dynamics code FLUENT (Ansys-15). Pressure-outlet boundary conditions are used for

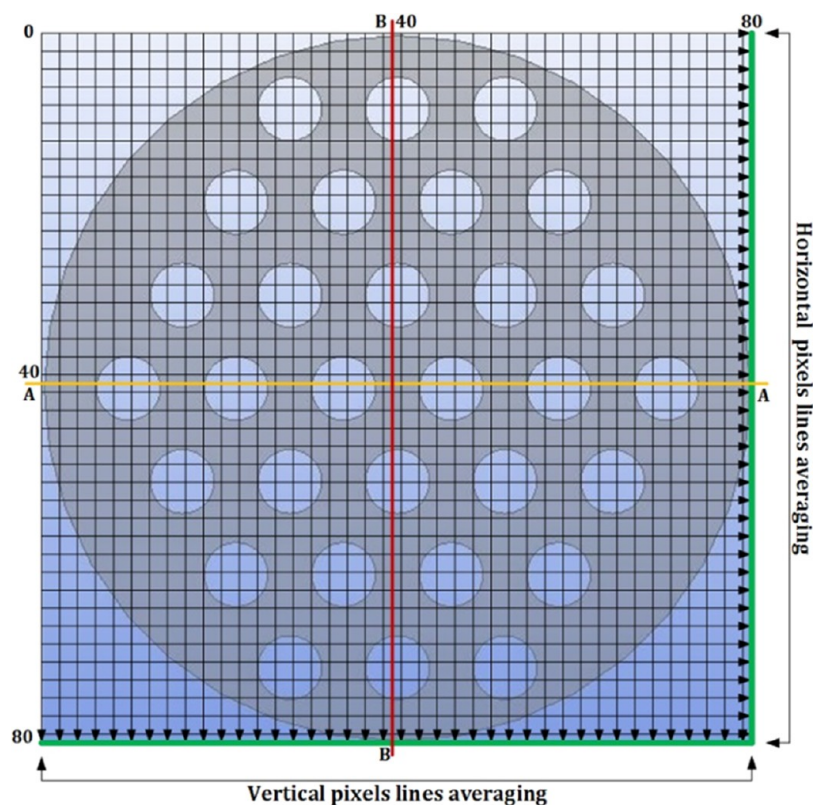


Figure 2. Imposing the bubble column with internals on 80×80 pixels used for CT image reconstruction (for clarity, it is plotted as 40×40 pixels where each pixel contains two pixels). The horizontal line (A–A) and vertical line (B–B) present the local gas holdup. Figure adapted from ref 41

the outlet surface of the bubble column (with and without internals), while the velocity condition has been applied for the inlet surface of the bubble column with a gas volume fraction equal to 1 due to the liquid phase in the bubble column of this study operating in batch mode. The no-slip boundary conditions are adapted along the walls, including the bubble column wall and the outside surface of internals. It is worth mentioning that the bubble column simulations during high superficial gas velocities ($U_g = 0.2$ and 0.45 m/s) encounter serious numerical problems. The dynamic liquid level was spilled out from the bubble column due to the large gas volume fraction gradient in the dynamic liquid level, where the same phenomenon was observed by Liang et al.⁶⁵ Thereby, a user-defined function (UDF) was implemented to increase the superficial gas velocity slowly and linearly with the simulation time to avoid the gas volume fraction from increasing rapidly. This (UDF) is inactivated when the superficial gas velocity reaches the needed velocity (0.2 or 0.45 m/s). The SIMPLE scheme has been used to solve the pressure–velocity coupling, while the second upwind scheme is used to solve the momentum and volume fraction equations. However, the type of grid used for the bubble column with and without internals is a hexahedral grid throughout the bubble column with internals, as shown in Figure 1. The numbers of the final grid for the bubble with and without internals are 694,930 and 430,331 cells, respectively. Furthermore, due to the simulation, which has been conducted using the Eulerian–Eulerian approach, demarcating the magnitude of the time step is essential to prevent encountering some stability or convergence problems in the numerical solution. Therefore, the Courant–Friederichs–Levy (CFL) condition, as given in eq 45, was applied to calculate the time step

$$C = \frac{u_y \Delta t}{\Delta y} \leq 0.125 \quad (45)$$

where C , u_y , Δy , and Δt are the Courant number, superficial gas velocity in a y -axial direction (m/s), cell size in a y -axial direction (m), and time step (s), respectively. Hence, the time step was varied according to the superficial gas velocity. However, in this study, the time step of 0.001 (s) has been used for all CFD simulations.

3. EXPERIMENT SETUP FOR CFD VALIDATION

The bubble column with and without internals that is simulated in this work by CFD with the earlier listed models and closures is 1.83 m in height and 0.14 m in inner diameter. Three arrangement types of internals have been used to simulate the internal effect, hexagonal arrangement, circular arrangement of 0.5 in. tube diameter, and circular arrangement of 1 in. tube diameter as illustrated in Figure 1b–d, respectively. More details about the bubble column and the internal arrangements were explained in Sultan et al.^{66,67} and Al Mesfer et al.⁴¹ The superficial gas velocity was calculated based on the free cross-sectional area (CSA) for the flow column, which varied from 0.05 to 0.45 m/s. Therefore, the initial liquid level was adjusted, with a simulation time of 0.0 (s) for each superficial gas velocity used to maintain the dynamic liquid level at the desired height.

Al Mesfer et al.⁴¹ investigated the impact of the internals on the gas holdup profiles using the CT technique. The gas holdup measurements were conducted at level $L/D = 5.2$. The data processing of the scan cross section was divided into 80×80 pixels. Therefore, the measured gas holdup profiles are exhibited using two methods local profile (lines A–A and B–B as shown in Figure 2)⁴¹ and lines averaged of the horizontal pixels and the

vertical pixels (the green lines in Figure 2). According to Al Mesfer et al.,⁴¹ results of these different methods of the gas holdup representation exhibited a significant difference in the gas holdup profiles for the same operating conditions. Thereby, Sultan et al.^{66–67,68} suggested that demonstrating the azimuthally time-averaged cross-sectional gas holdup distribution would provide quantifiable and easy-to-understand results.

Furthermore, to determine the azimuthally averaged profiles, a method was developed by Sultan et al.⁶⁹ to divide the CT reconstructed image (80 × 80 pixels) in half (left and right of 40 × 40 pixels) and then averaged them separately to achieve a clearer representation of the results. Therefore, the CFD simulation data obtained in this study have been extracted and processed using the same method of azimuthally time averaging. Finally, the results have been directly compared with the experimental results to properly assess the CFD simulation validation.

4. RESULTS AND DISCUSSION

4.1. Numerical Simulation Sensitivity. The grid size is a critical factor in solving the governing equations of CFD simulation. A well-orthogonal grid influences the numerical solution regarding the instability and lack of convergence.⁴⁹ Therefore, testing five different grid sizes so that their specifications are listed in Table 1 has been accomplished as a

Table 1. Grid Size Specifications

type	dimensions	type	no. of cells
A	$\Delta y = 0.01$	Sweep/O-grid	47,223
B	$\Delta y = 0.0067$	Sweep/O-grid	167,300
C	$\Delta y = 0.005$	Sweep/O-grid	430,331
D	$\Delta y = 0.004$	Sweep/O-grid	880,992
E	$\Delta y = 0.0033$	Sweep/O-grid	1,569,683

first step. Figure 3 illustrates the effect of the grid size on the azimuthally time-averaged cross-sectional gas holdup distribution that was obtained at $L/D = 5.2$. The variation in the azimuthally time-averaged cross-sectional gas holdup is affected by the grid size and is demarcated by calculating the average absolute relative difference (AARD) compared to the experimental results, as given in eq 46

$$\text{AARD} = \frac{1}{N} \sum_N \left| \frac{\epsilon_{i,\text{experiment}} - \epsilon_{i,\text{grid}}}{\epsilon_{i,\text{experiment}}} \right| \quad (46)$$

Thereby, the variations in the AARD between the experiment data of Al Mesfer et al.⁴¹ and the five sizes of grid types A, B, C, D, and E are 30.2, 19.5, 20.3, 19.9, and 20.1%, respectively. Accordingly, the average absolute relative difference (AARD) of the grid types (B–E) is insignificant. Therefore, type B has been utilized in all of the simulations for the validation and internal effect study.

As long as the numerical simulation for the multiphase flow in the bubble column has utilized the Eulerian–Eulerian approach, solving the governing equations in time-dependent is essential to avoid the instability and the divergence. Consequently, demarcating the steady-state or the pseudo-steady-state condition of the system is important to start the time-averaged solution. Figure 4 illustrates the area-weighted average of the local gas holdup in the central region and at $L/D = 5.2$ as a function of time. As shown in Figure 4, the time average of the local gas holdup no longer significantly varies with time after 30,

60, and 100 (s) for the superficial gas velocity of 0.05, 0.2, and 0.45 m/s, respectively. The difference in the time needed to reach the steady state for each superficial gas velocity used was attributed to the use of the (UDF) for the high superficial gas velocity (0.2 and 0.45 m/s), and hence, the numerical solution keeps unsteady until the (UDF) reaches the needed superficial gas velocity value. Therefore, it can be concluded that after the initial transition of about 30, 60, and 100 (s) for superficial gas velocities of 0.05, 0.2, and 0.45 m/s, respectively, the pseudo-steady-state condition has been established.

The flow in the bubble column is classified as chaotic.^{9,70,71} Hence, the numerical results have been exhibited in the time-averaged sense, which were extracted after 30, 60, and 100 (s) for the superficial gas velocities 0.05, 0.2, and 0.45 m/s, respectively, after the start of the simulation. Accordingly, in this study, the time needed to collect data in a time-averaged sense has been defined as duration-time-averaged. The effect of the duration-time-averaged gas holdup distribution is worth considering. Figure 5 shows the time-averaged cross-sectional gas holdup distribution for different duration-time-averaged for the simulation of the bubble column without internals at $U_g = 0.2$ m/s. The variation in the duration-time-averaged exhibits a slight effect on the time-averaged gas holdup distribution, where the (AARD) varied in a range (1.02–2.9)%, which is attributed to avoiding the unsteady-state time zone. However, in this work, a duration-time-averaged of 60 (s) has been used.

4.2. Assessing the Validation of the Interfacial Forces and the Population Bubble Model (PBM). The gas holdup distribution is a key parameter in the bubble column reactors, where the radial variation in the gas holdup leads to the liquid circulation, which results in demonstrating the mixing rate and the heat and mass transfer.^{12,65,72} Thereby, a gas holdup was used to validate the simulation results of this study.

4.2.1. Drag Force. The drag force, among all of the interfacial forces, dominants the prediction of the hydrodynamics in the bubble column,^{73,74} and if appropriately validated, the entire interfacial forces would be validated correctly. The effect of different models of the drag force on the prediction of the time-averaged gas holdup distribution and its comparison with the experimental results of Al Mesfer et al.⁴¹ at the gas velocity $U_g = 0.08$ m/s based on the free cross-sectional area for flow is illustrated in Figures 6 and 7. The simulation results in Figure 6 show that the azimuthally time-averaged gas holdup radial profiles for all different models exhibit a semiflat distribution, which is attributed to the drag force being the only interfacial force used in Figure 6, particularly in the wall region ($r/R = 0.66–1$). The average absolute relative difference (AARD) between the model predictions of Grace et al.,⁵¹ Tomiyama,⁵² Morsi and Alexander,⁵³ and Schiller and Naumann⁵⁴ and the experimental results are 20.8, 18, 30.4, and 28.2%, respectively. The Grace et al.⁵¹ and Tomiyama⁵² models give the closest prediction for the experimental results despite the fact that the predictions do not follow the trend of the experimental radial profile. Hence, these models are used for the next steps of validation. Furthermore, the CFD images of the same scale as CT images for the time-averaged cross-sectional gas holdup distribution at $H/D = 5.2$ are illustrated in Figure 7. These results depict significant differences in the prediction of gas-phase holdup distribution with the experimental results. This is due to using only the drag force, which is not adequate for simulating the hydrodynamics in the bubble column, particularly in the wall region.

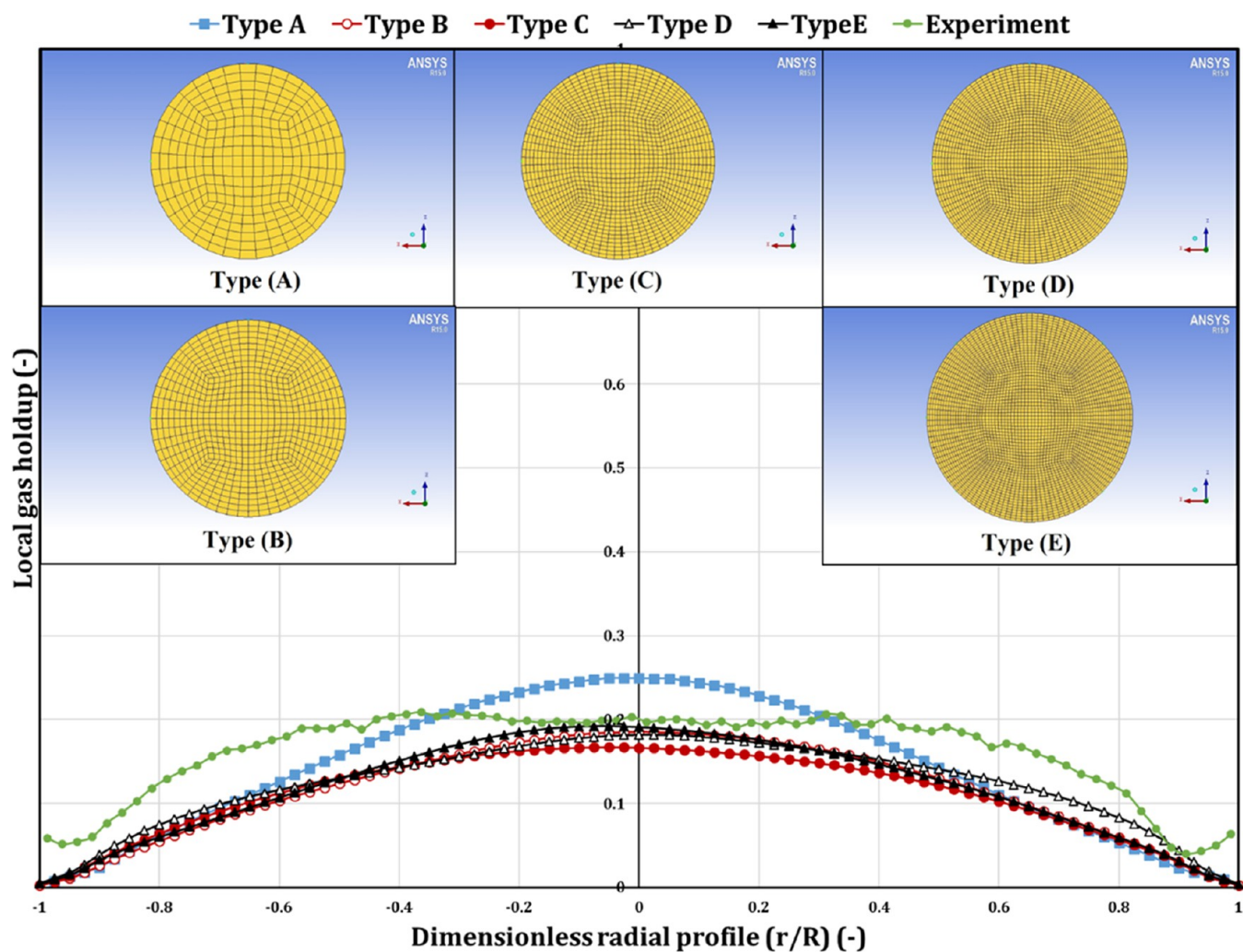


Figure 3. Effect of the grid size (types A, B, C, D, and E) on the azimuthally averaged gas holdup profiles in comparison with the experimental results for $U_g = 0.05$ m/s.

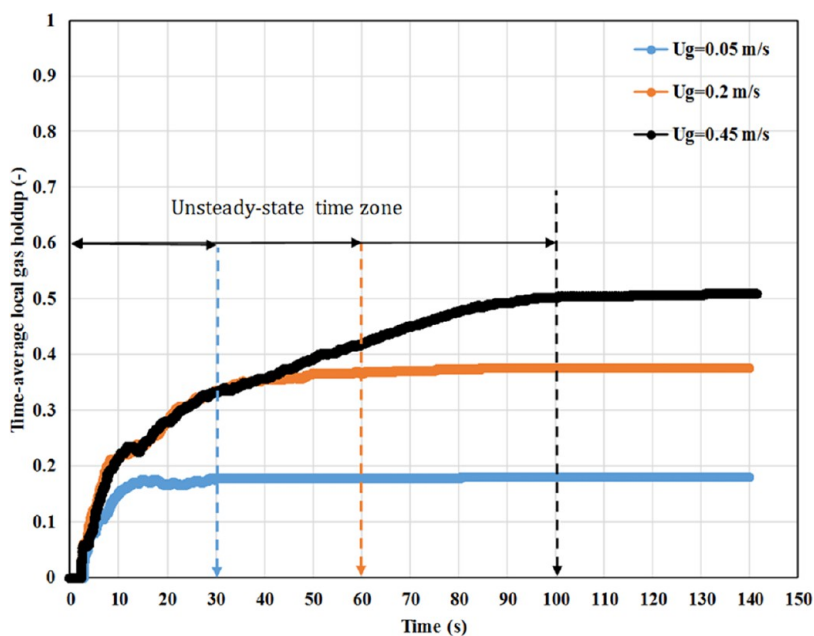


Figure 4. Variation of area-weighted averages of the local gas holdup with time in the bubble column without internals.

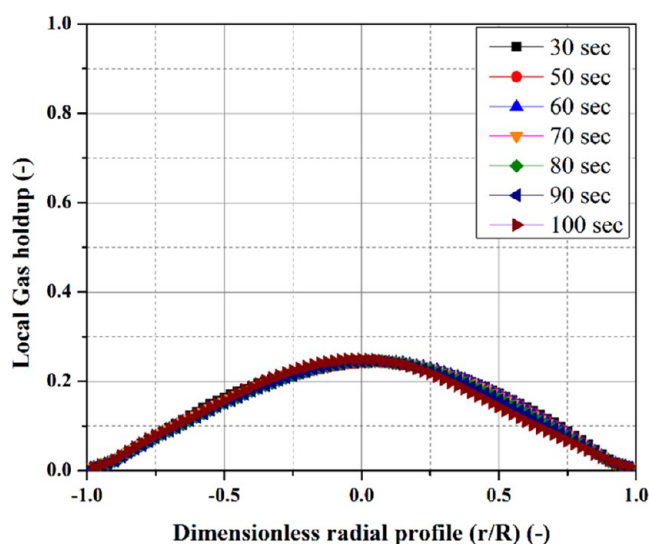


Figure 5. Effect of the time collection on the time-averaged cross-sectional gas holdup distribution at $U_g = 0.2$ m/s.

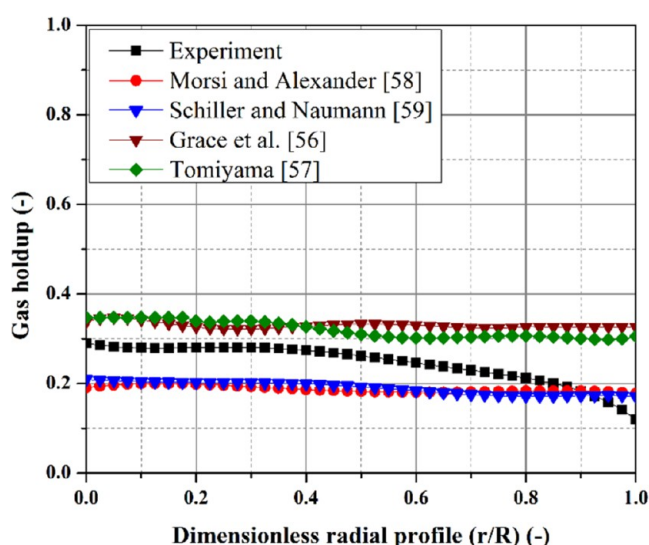


Figure 6. Drag force effect on the simulation results of the bubble column without internals.

4.2.2. Wall Lubrication. In this part, the drag force, Grace et al.⁵¹ and Tomiyama⁵² models, was combined with the wall lubrication force to assess the validation of the wall forces using three models, which are Antal et al.,⁵⁸ Tomiyama,⁵² and Frank et al.,⁵⁹ with the default set of coefficient values that are given in eqs 27–30. The simulation results with all wall lubrication models evaluated are shown in Figure 8 to illustrate the effect of the wall lubrication force and the model used on the azimuthally time-averaged gas holdup radial profile. As shown in Figure 8, the impact of the wall lubrication with different models is significant in enhancing the drag force performance and the prediction of the wall region. The prediction of the wall of this region was not satisfying due to using a constant bubble size $d_B = 5$ mm; the trend of the radial profile prediction has improved. The average absolute relative difference (AARD) values for Grace et al.⁵¹/Antal et al.,⁵⁸ Grace et al.⁵¹/Tomiyama,⁵² Grace et al.⁵¹/Frank et al.,⁵⁹ Tomiyama⁵²/Antal et al.,⁵⁸ Tomiyama/Tomiyama,⁵² and Tomiyama⁵²/Frank et al.⁵⁹ models are 17, 29.6, 35.3, 42.2, 39.1, and 37.3%, respectively. The drag force model of Grace et al.⁵¹

and the wall lubrication model of Antal et al.⁵⁸ give better predictions in terms of the least and closer trend AARDs. Hence, these models have been selected for the next steps of validation and in the current study.

4.2.3. Turbulent Dispersion. The predictions of two turbulent dispersion force models described in eqs 32 and 34 were compared with the experimental results. The two models of turbulent dispersion have been tested with default coefficients listed in eqs 32 and 34 along with the combination of the drag force and the wall lubrication force that were represented by Grace et al.⁵¹ and Antal et al.,⁵⁸ respectively. The effect of these models of the turbulent dispersion force on a simulation of the radial profile of gas holdup is illustrated in Figure 9. The simulation results of Simonin and Viollet⁶⁰ are in good agreement with the experimental data in the central region of the column compared to those of the Burns et al.⁶¹ model, which gives underestimated predictions with AARD = 22% and 29%, respectively. However, close to the wall region, a significant difference exists between Simonin and Viollet⁶⁰ model predictions and experimental results. The simulation results of Simonin and Viollet⁶⁰ and Burns et al.⁶¹ models with their default coefficient values still give predictions less than the experimental results in the wall region of the azimuthally time-averaged gas holdup radial profile. This could be attributed to the absence of the effect of the lift force.

4.2.4. Lift Force. Tabib et al.⁷⁵ concluded while analyzing the interfacial forces and turbulent models in the 3D CFD simulation of the bubble column that the positive value of the lift force coefficient C_l would make the bubbles concentrate toward the wall region of the bubble column (i.e., leads to a flatter gas holdup profile). Therefore, the magnitude of the coefficient will depend on the bubble size. Tabib et al.⁷⁵ reported that $C_l = -0.2$ gives a good agreement with the experimental results. In this work, the experimental results used show the gas holdup in a parabolic profile (i.e., high gas holdup in the central region of the bubble column). Hence, $C_l = -0.2$ has been used in this study along with a combination of the drag force, the wall lubrication force, and the turbulent dispersion force that were represented by Grace et al.,⁵¹ Antal et al.,⁵⁸ and Simonin and Viollet,⁶⁰ respectively. Figure 10 illustrates the effect of the lift force on the simulation results of the azimuthally time-averaged gas holdup profiles. The trends and the magnitudes of the gas holdup in Figure 10 show that using a constant lift force coefficient improves the simulation results with a diversion of AARD = 17%, although it underestimates the experimental results, particularly in the wall region. Since the lateral lift force presents the migration of bubbles toward the bubble column center or wall regions based on the bubble size, the lift force becomes the administrating force to control the gas holdup distribution.⁷⁶ Thereby, as long as one bubble size is assumed in the simulation, it is hard for the prediction results to converge with the experimental results, particularly in the wall region.

4.2.5. Population Bubble Model (PBM). As shown earlier in assessing the interfacial forces for gas holdup predictions, the performance prediction of these forces is governed by the bubble size. The flow in the bubble column is complex as a result of the complex interaction between the phases and the momentum transferring across the gas–liquid interface surface, which are controlled by the bubble size. Therefore, using the population bubble model (PBM) to predict the bubble size could improve the CFD predictions in capturing the hydrodynamics of the bubble column, especially in the turbulent flow regime, where the bubbles prevail over a wide range of sizes. In this study, Luo–

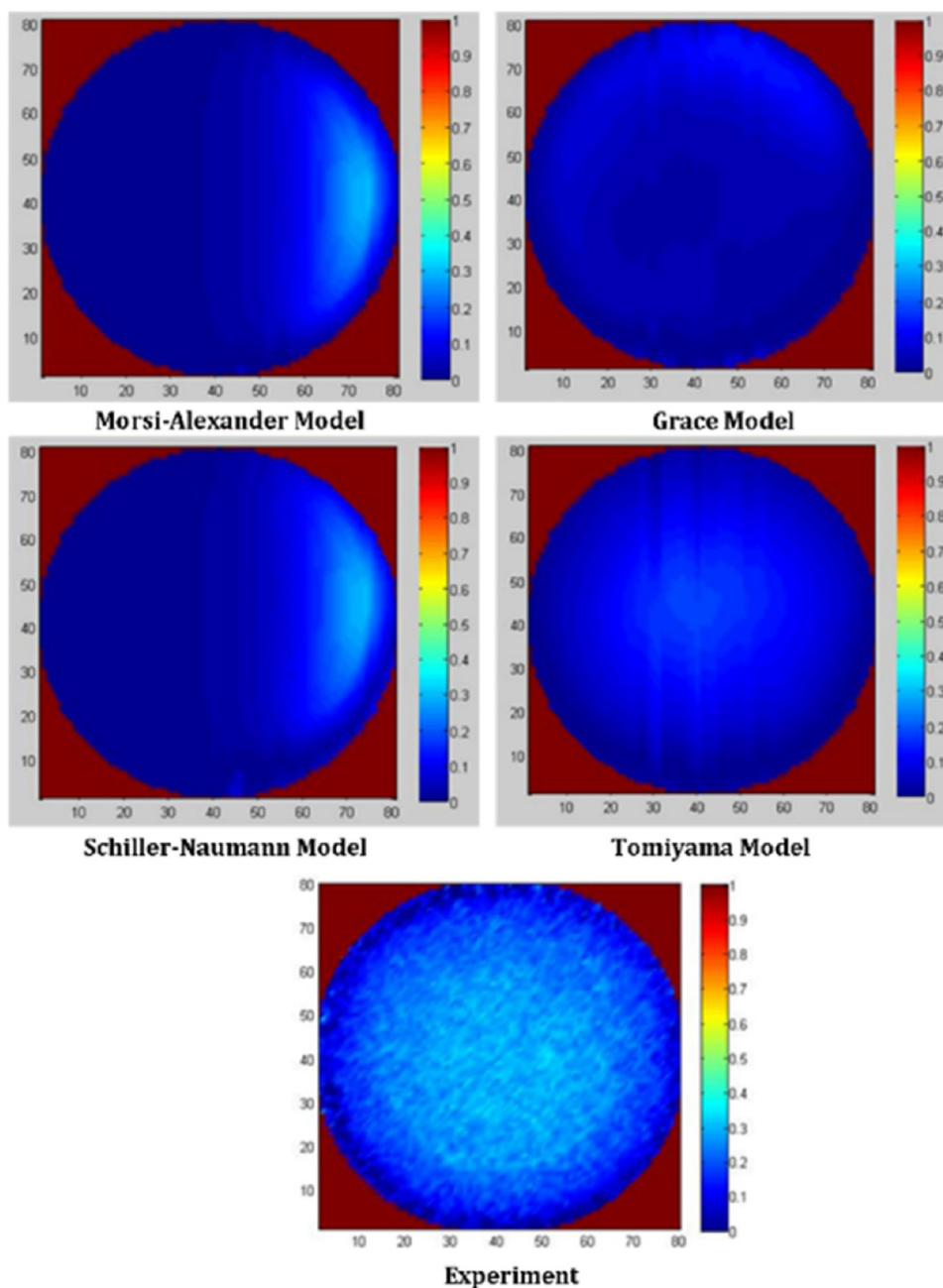


Figure 7. CFD simulation images of the cross-sectional time-averaged gas holdup for the bubble column without internals, $U_g = 0.08$ m/s.

Luo models have been used for the coalescence and the breakup rates. Figure 11 illustrates the effect of using the population bubble model (PBM) incorporated with validated models of the interfacial forces on the simulation results of the azimuthally time-averaged gas holdup distribution. The simulation results appear to agree well with the experimental data with a percentage of the averaged absolute relative difference of about (AARD) = 5.8%. This reflects the capability of the PBM in improving the CFD simulation predictions. Chen et al.⁷⁷ implemented the bubble population balance equation (BPBE) using two numbers of bubble groups (9 and 16 classes) to simulate the bubble column in two and three dimensions operated over a range of superficial gas velocity ($U_g = 0.08$ to 0.2 m/s). Their results revealed that the incorporation of the BPBE is critical to capture the gas holdup faithfully, and using nine groups of bubble size is sufficient. Recently, Kagumba and

Al-Dahhan³⁶ measured the bubble properties in an experimental setup of a bubble column with and without internals, which is the same as that used in this simulation study, in terms of the size of the bubble column and the internals. Accordingly, the data obtained by Kagumba and Al-Dahhan³⁶ regarding the bubble size has been utilized in this study to optimize the numbers of the bubble groups.

Five bubble groups (5, 10, 15, 20, and 25), listed in Table 2, have been used to solve the population bubble model (PBM). The simulation results of the effect of different numbers of bubble groups on the azimuthally time-averaged gas holdup are illustrated in Figure 12. The obtained results show that the variation in the numbers of bubble groups has a significant effect on the simulation results, with a percentage of an averaged absolute relative difference (AARD) of 39.45, 33.62, 37.1, 16.8, and 16.6% for the used bubble groups of 5, 10, 15, 20, and 25,

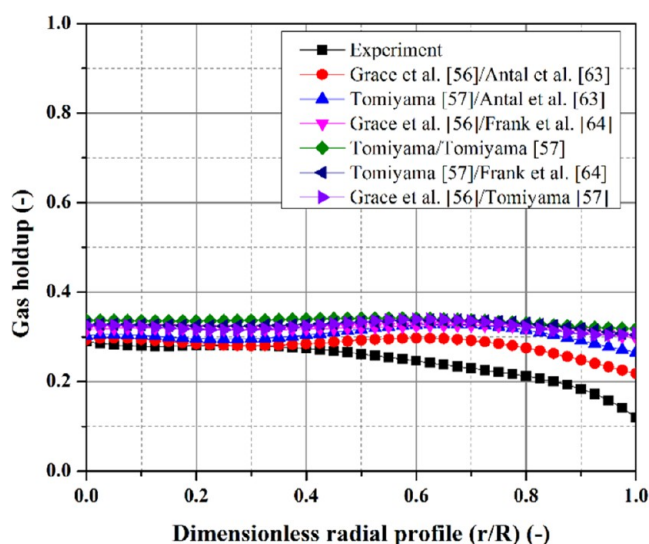


Figure 8. Wall lubrication force simulation results of the bubble column without internals.

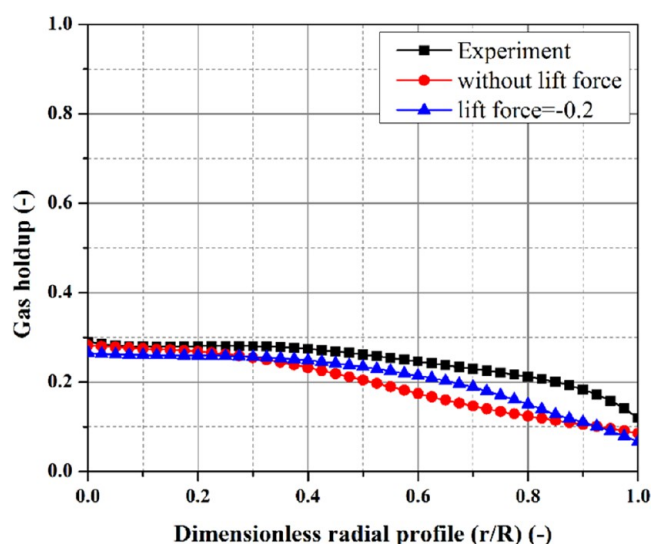


Figure 10. Lift force effect on the simulation results of the bubble column without internals.

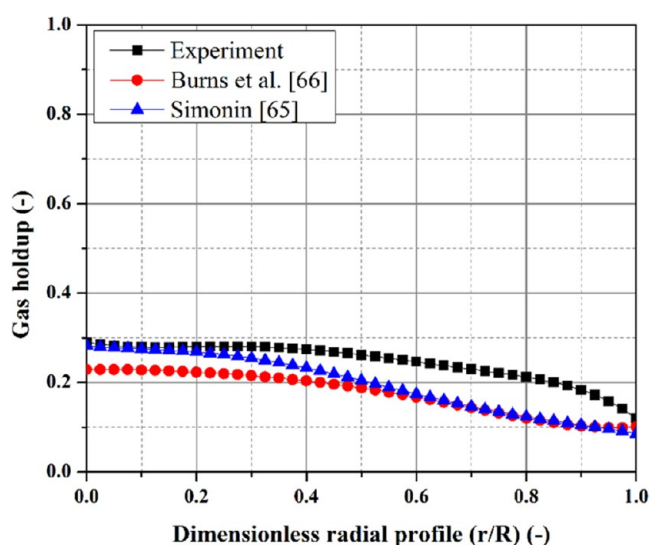


Figure 9. Turbulent dispersion force effect on the simulation results of the bubble column without internals.

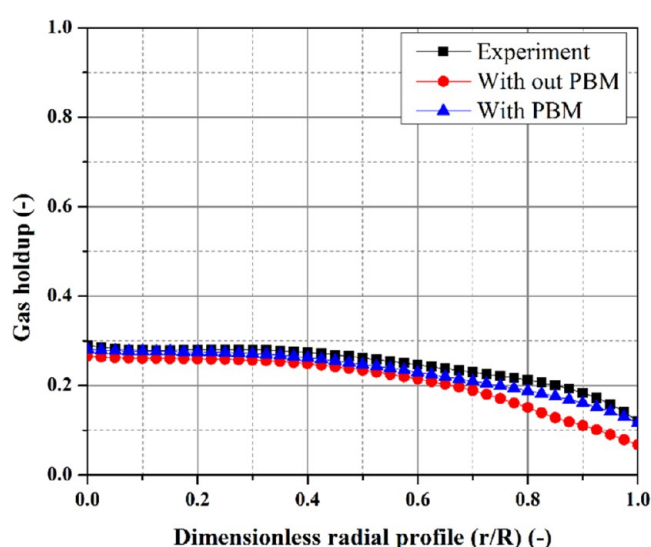


Figure 11. Population bubble model (PBM) effect on the simulation results of the bubble column without internals.

respectively. It seems that there is no significant variation in the prediction of group numbers 20 and 25. Therefore, group number 20 has been used for the CFD simulation for the superficial gas velocity of $U_g = 0.2$ and 0.45 m/s (churn turbulent flow regime), whereas bubble group number 10 has been used for the simulation under the operating condition of the superficial gas velocity of $U_g = 0.05$ m/s (bubbly flow regime).

4.3. Turbulent Model Assessment. Two models of turbulent kinetics, which are standard ($k - \epsilon$) and RNG ($k - \epsilon$), have been assessed along with the other selected models and closure as shown in Figure 13 with the experimental results of the liquid velocity of Al Mesfer et al.⁷⁸ The simulation results of the two models are illustrated in Figure 13. As shown, the RNG ($k - \epsilon$) model exhibits a good matching to the experimental results for the liquid velocity with AARD = 17.6%, in particular, in the central and the wall regions of the bubble column and for the reflecting point that is located at $r/R \sim 0.69$, whereas the standard ($k - \epsilon$) model exhibits poor predictions in these regions. The renormalization group (RNG) model accounted

for the effect of the small-scale turbulence by means of a random forcing function in the momentum equation. Hence, the renormalization group (RNG) model systematically removes scales of motion from the governing equations by expressing their effects in terms of larger-scale motions and a modified viscosity. However, the standard ($k - \epsilon$) model uses the small eddies in defining the large eddies scale, which, in turn, reduces the efficiency of this model at high Reynolds numbers (i.e., high superficial gas velocity).^{44,79} Therefore, the standard ($k - \epsilon$) model is restricted to the flow without internal geometries inside the simulated field. Accordingly, the RNG ($k - \epsilon$) model is recommended as long as the current work aims to study the effect of internals at the churn turbulent flow regime.

4.4. Effects of Superficial Gas Velocity on the Validation of the 3D CFD Simulations. Figures 14a–c and 15a–c illustrate the 3D CFD simulation results of the azimuthally time-averaged gas holdup distribution profile along with the experimental results reported by Sultan et al.⁶⁷ in a bubble column without internals and a bubble column with

Table 2. Bubble Group Numbers

5 groups classes index	1	2	3	4	5																
d_b , mm	1.3	2.6	5.1	10.2	20.2																
10 groups classes index	1	2	3	4	5	6	7	8	9	10											
d_b , mm	1.3	1.76	2.4	3.3	4.4	5.97	8.1	11	14.9	20.2											
15 groups classes index	1	2	3	4	5	6	7	8	9	10	11	12	13	14	15						
d_b , mm	1.3	1.6	1.9	2.3	2.9	3.5	4.2	5.2	6.3	7.6	9.3	11.3	13.7	16.7	20.3						
20 groups classes index	1	2	3	4	5	6	7	8	9	10	11	12	13	14	15	16	17	18	19	20	
d_b , mm	1.3	1.5	1.74	2	2.3	2.67	3.1	3.57	4.13	4.8	5.5	6.36	7.35	8.5	9.81	11.3	13.1	15.1	17.5	20.2	
25 groups classes index	1	2	3	4	5	6	7	8	9	10	11	12	13	14	15	16	17	18	19	20	
d_b , mm	1.3	1.46	1.64	1.84	2.06	2.3	2.6	2.92	3.3	3.67	4.13	4.6	5.2	5.83	6.55	7.35	8.3	9.26	10.4	11.7	
classes index	21	22	23	24	25																
d_b , mm	13.1	14.7	16.5	18.5	20.8																

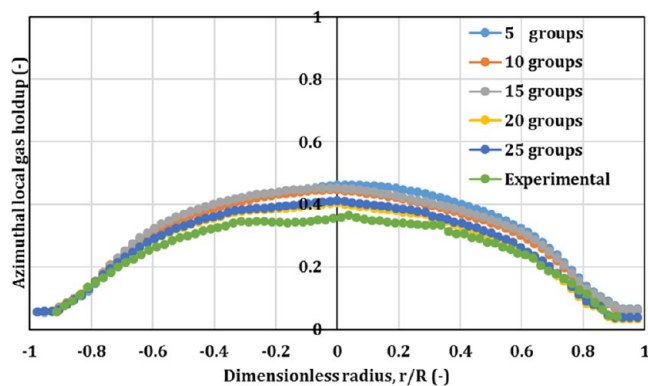


Figure 12. Effect of the group numbers of bubbles on the simulation results of gas holdup in the bubble column without internals at $U_g = 0.2$ m/s.

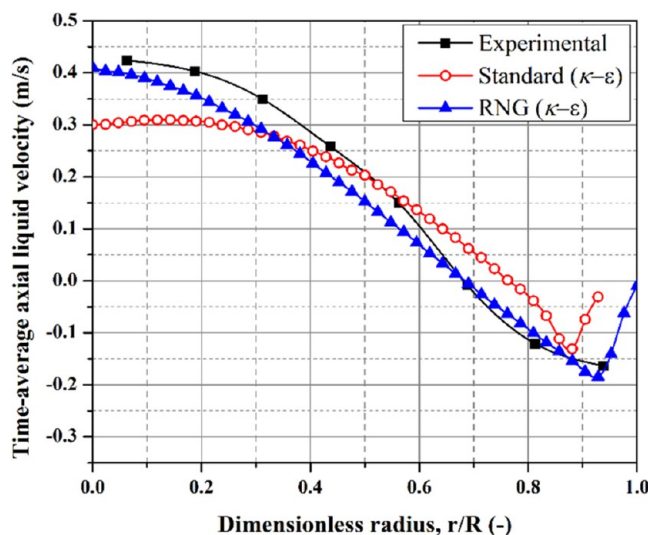


Figure 13. Effect of turbulent kinetic energy models on the time-averaged axial liquid velocity (m/s) compared with the experimental results.

internals, respectively. The validation for the bubble column without internals shows that the percentages of the averaged absolute relative difference (AARD) between the simulation and the experimental results at superficial gas velocities of 0.05, 0.2, and 0.45 m/s are about 14.6, 16.8, and 16.2%, respectively, while, in the case of the bubble column with internals, the absolute relative difference (AARD) is about 29.5, 24.8, and 15.9%, respectively. However, the reasonable agreement between the 3D CFD simulation results and the experimental data confirms the capability of the selected CFD closures in predicting the hydrodynamics of the bubble column in the bubbly flow and churn turbulent flow regimes. This has been attributed to two reasons for coupling the Eulerian–Eulerian approach with the population bubble model (PBM) and using the bubble group numbers that cover all of the bubble sizes that were measured in the experiment.

To demonstrate the effect of the superficial gas velocity on the azimuthally time-averaged gas holdup diameter profiles in the bubble column without internals, the CFD simulation results are plotted in Figure 16. As the superficial gas velocity increases, the magnitude value of the time-averaged gas holdup increases along with the radial position. However, the gas holdup magnitude value at the central region of the bubble column is about 0.2 at

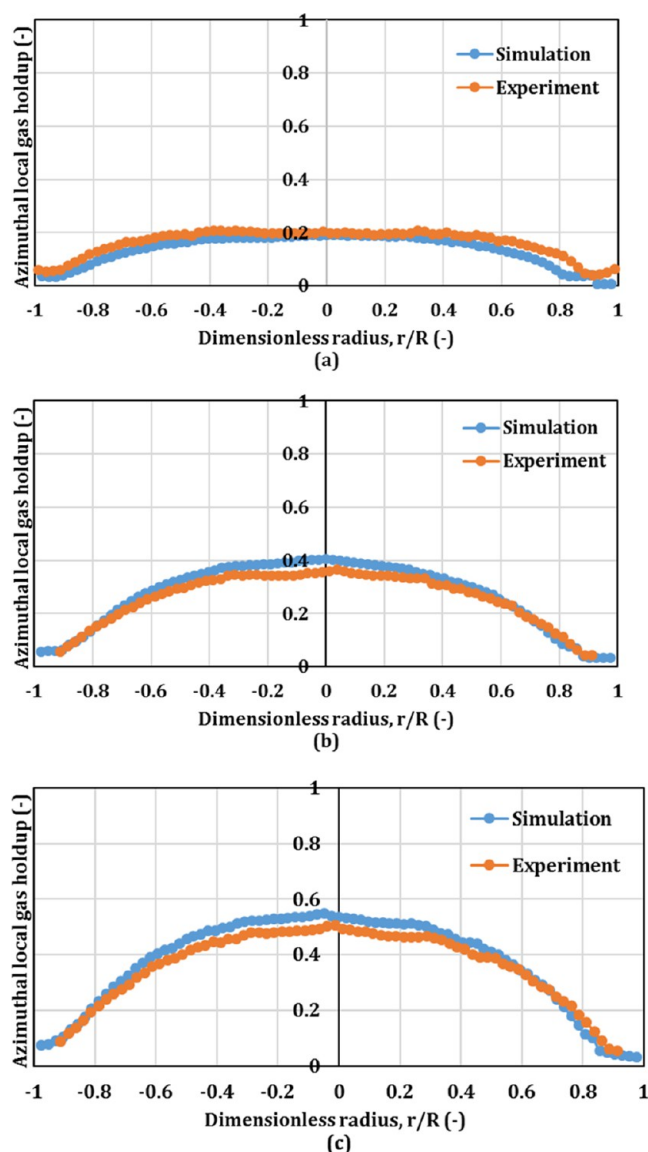


Figure 14. Validating the 3D CFD simulation results with experimental data of Sultan et al.⁶⁶ for the azimuthally time-averaged diameter profiles of gas holdup in the bubble column without internals: (a) $U_g = 0.05$ m/s, (b) $U_g = 0.2$ m/s, and (c) $U_g = 0.45$ m/s.

0.05 m/s. The superficial gas velocity increases from 0.05 to 0.2 m/s and 0.45 m/s and the gas holdup increases by 51% and 63%, respectively. It is worth noting that the simulation results of the gas holdup at the low superficial gas velocity of $U_g = 0.05$ m/s of the bubbly flow regime show that the region close to the wall has a larger gas holdup effect than that at higher velocities. The simulation results qualitatively agree with the results reported by Kagumba and Al-Dahhan,³⁶ Kumar,⁸⁰ Rados et al.,⁸¹ and Nedeltchev and Shaikh.⁸² Figure 16 clearly exhibits that the azimuthally time-averaged gas holdup has a smooth profile with a parabolic shape. The maximum magnitude of the gas holdup is in the central region of the bubble column and progressively decreases toward the wall. This phenomenon can be attributed to gas bubbles accumulating at the core of the column, where there is less shear stress than near the wall. This parabolic profile of the gas holdup leads to the gross liquid circulation throughout the column, with the liquid flowing up in the central region and down near the wall.⁸³

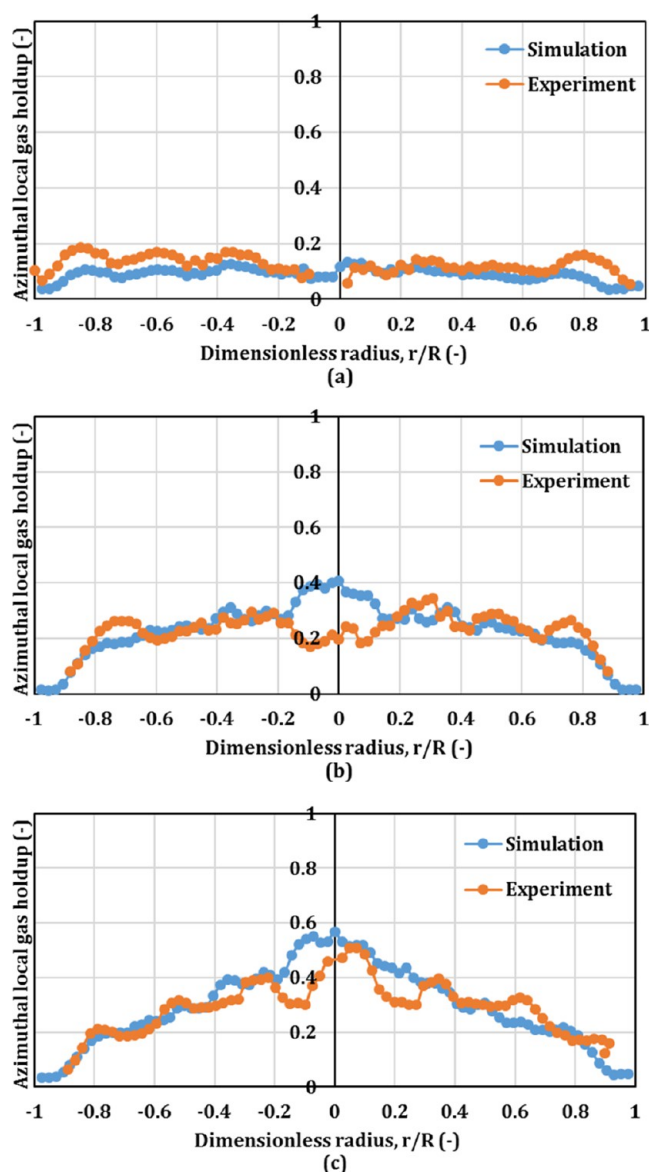


Figure 15. Validating the 3D CFD simulation results with experimental data of Sultan et al.^{3,4} for the azimuthally time-averaged diameter profiles of gas holdup in the bubble column with internals of hexagonal arrangement: (a) $U_g = 0.05$ m/s, (b) $U_g = 0.2$ m/s, and (c) $U_g = 0.45$ m/s.

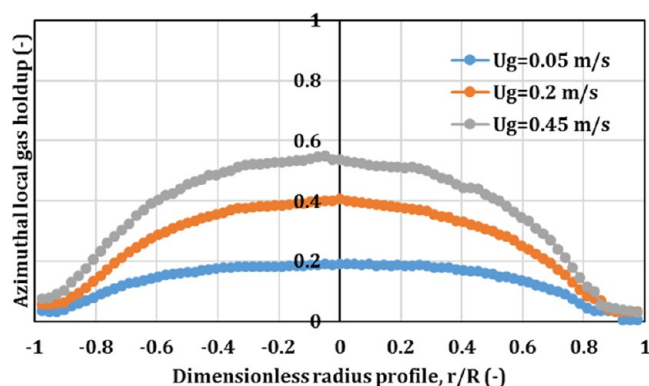


Figure 16. Effect of the gas velocity on the azimuthally time-averaged gas holdup diameter profiles in the bubble column without internals.

The effect of the superficial gas velocity, calculated based on the free cross-sectional area (CSA) for the flow inside the column, on the azimuthally time-averaged gas holdup diameter profile of the bubble column in the presence of internals is illustrated in Figure 17. A similar trend was found as the gas

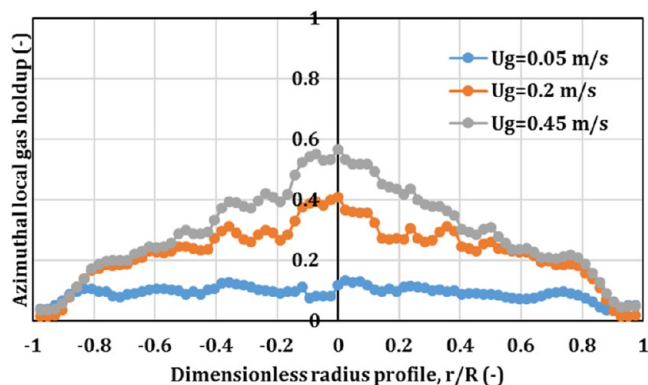


Figure 17. Effect of the gas velocity based on the free cross-sectional area for the flow inside the column on the azimuthally time-averaged gas holdup diameter profile in the bubble column with internals.

holdup magnitudes at the central region of the bubble column are about 0.19 at $U_g = 0.05$ m/s, and with increasing the gas velocity from 0.05 to 0.2 and 0.45 m/s, the gas holdup increases by 66% and 78%, respectively. The magnitudes of the gas holdup in the wall region exhibit an insignificant change by increasing the superficial gas velocity.

4.5. Effect of the Presence of Internals on the Gas Holdup. Figure 18 illustrates the effect of the gas velocity and

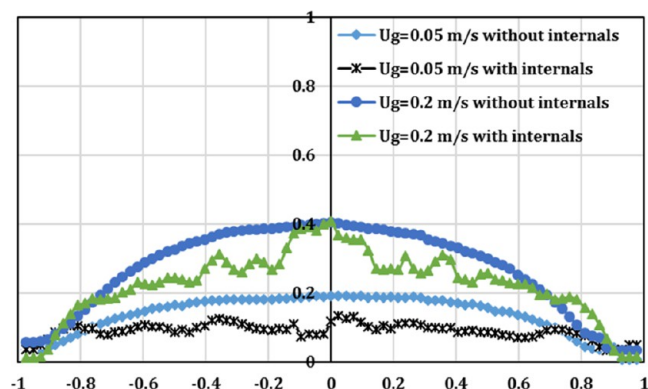


Figure 18. CFD results of the effect of the presence of internals on the azimuthally time-averaged gas holdup diameter profile at $U_g = 0.05$ and 0.2 m/s calculated based on the free cross-sectional area for the flow inside the column.

the presence of internals, with a hexagonal configuration, on the azimuthally time-averaged gas holdup diameter profile in the bubble column with and without internals. The superficial gas velocities of $U_g = 0.05$ and 0.2 m/s are calculated based on the free cross-sectional area (CSA) for the flow inside the column, corresponding to the bubbly flow and the churn turbulent flow regimes, respectively. As shown, the gas holdup profiles in the bubble column with internals are slightly affected by the presence of internals. This is attributed to the fact that gas velocities have been calculated based on the free cross-sectional area (CSA) for the flow inside the column. Hence, the mass flow rate of the gas phase is less than that in the column without

internals to a certain extent. This finding agrees with the results reported by Al Mesfer et al.,¹ Kagumba and Al-Dahhan,²⁹ and Sultan et al.⁶⁶

Furthermore, as shown in Figure 18, the presence of internals significantly alters the gas holdup profiles from a smooth parabolic shape for the bubble column without internals to wavy line profiles in the bubble column with internals. This phenomenon has been attributed to the occupying cross section of the bubble column by the internals. Thereby, the internal tubes control the distribution of the bubbles through the cross section of the bubble column. Therefore, the variation in the shape of gas holdup profiles is related to the numbers of internal tubes, the gaps between the tubes, and the size of the internal tubes.

It is worth noting that in Figures 17 and 18, as the superficial gas velocity increases, the gas holdup profiles become steeper and most of the gas fraction concentrates in the central region of the bubble column, while there is no significant change in the wall region. The enhancement in the gas holdup at the central region could be attributed to the movement of large bubbles, in the absence of internals, toward the low shear stress region (i.e., in the center of the bubble column and away from the wall of the bubble column). Hence, the large bubble sizes accumulate in the central region of the bubble column. While in the presence of internals, the movement of the bubbles is controlled via the hindrance offered by the tubes against the bubble movement. Figure 19a–f depicts the CFD cross-

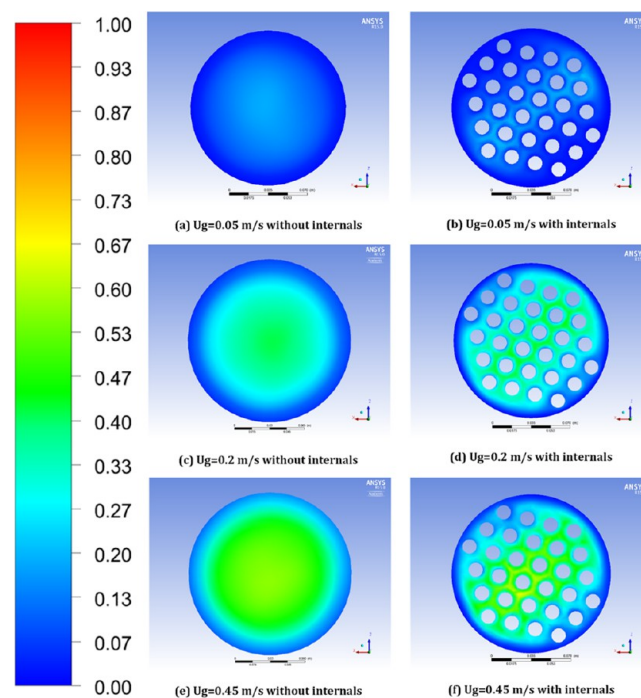


Figure 19. CFD cross-sectional distribution of the time-averaged gas holdup at varying gas velocities calculated based on the free cross-sectional area (CSA) of the bubble column with and without internals.

sectional distribution of the time-averaged gas holdup in the bubble column with and without internals at different superficial gas velocities of $U_g = 0.05$, 0.2, and 0.45 m/s. The variations in the color indicate the alteration in the magnitudes of the time-averaged local gas holdup. Figure 19 clearly illustrates that the variation in the gas holdup distribution over the cross section of the bubble column is affected by the presence of internal gas and

the superficial gas velocity. The same phenomenon has been reported by Al Mesfer et al.,¹ Sultan et al.,⁴ and Agahzamin and Pakzad.⁴³

4.6. Effect of the Internal Configurations and the Internal Size on the Time-Averaged Gas Holdup. The effect of the internal configurations on the time-averaged gas holdup distribution and diameter profiles has been demonstrated by the CFD results at the superficial gas velocity $U_g = 0.2$ m/s. Two arrangements of hexagonal and circular for this purpose were used, which occupy the same cross-sectional area (CSA) of the column and the same internal tube size of 0.5 in. The CFD simulation results of the bubble column equipped with the circular configuration compared with the experimental results are illustrated in Figure 20. The comparison shows that

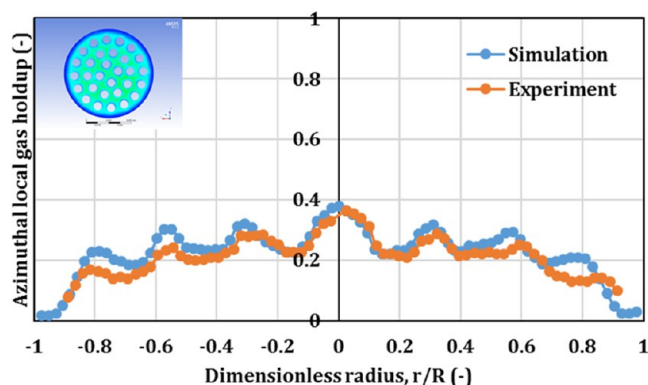


Figure 20. Validation of the CFD simulation results of the bubble column equipped with internals with a circular configuration of 0.5 in. diameter.

the simulation results reasonably agree with the experimental data with a percentage of the averaged absolute relative difference of about (AARD) = 20.4%.

Figure 21 illustrates the effect of different configurations (i.e., hexagonal and circular) on the time-averaged gas holdup distributions. As shown, the bubble column with the hexagonal

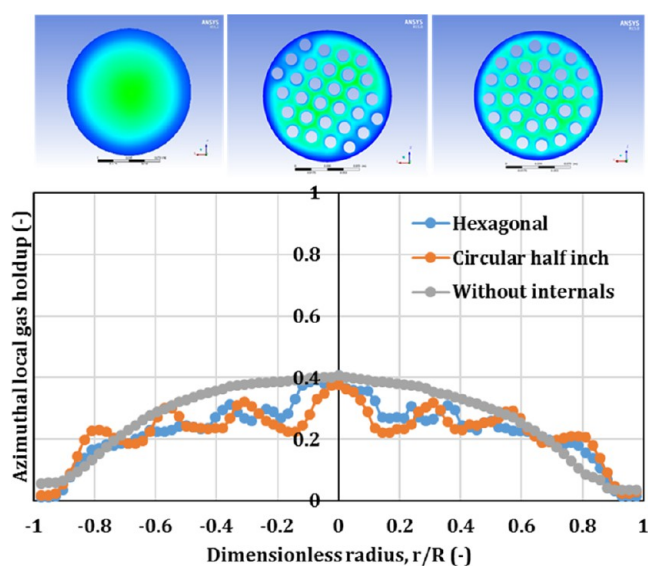


Figure 21. Effect of the internal configurations on the time-averaged gas holdup distribution without and with internals of 0.5 in. diameter at $U_g = 0.2$ m/s.

and circular configurations of tubes exhibits a uniform gas holdup profile with a remarkable increase in the magnitudes of the gas holdup in the central region of a dimensionless radius $r/R = 0.0-0.8$ compared to the wall region of about 57 and 63% of hexagonal and circular configurations, respectively. Figure 21 further reveals that using internals with a hexagonal configuration shows a higher magnitude value of gas holdup than those with the circular configuration in the central region of the bubble column (i.e., dimensionless radius, $r/R = 0.2$ to -0.2). In addition, less gas holdup in the wall region compared to that in the circular configuration has been found. According to that, the internals of the circular arrangement exhibit a semiflat gas holdup profile, while the hexagonal arrangement provides a higher gas holdup in the central region of the column. These findings agree with the results that were reported by Sultan et al.⁶⁷ However, the change in the configuration of the internals would significantly influence the gas holdup profiles. These phenomena could be attributed to the variation in the space between the internal tube in the circular and hexagonal arrangements, which significantly affects the distribution of the bubble based on size.

The effect of the variation in the internal tube size on the time-averaged gas holdup distributions has been demonstrated by using CFD results in Figure 22 at a superficial gas velocity of $U_g =$

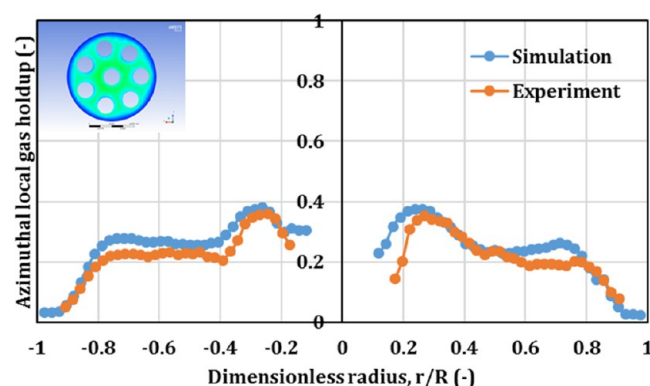


Figure 22. Validation of the CFD simulation results of the bubble column equipped by internals with a circular configuration of 1 in. tube size.

0.2 m/s. Two columns were used with one equipped with the internals of 0.5 in. diameter and the other equipped with the internals of 1 in. diameter. The CFD simulation of the bubble column with 1 in. diameter internals was validated against the experimental results that were reported by Sultan et al.,⁶⁶ as illustrated in Figure 22. The CFD simulation exhibits good agreement with the experimental data, with a percentage of the averaged absolute relative difference of (AARD) about 18.4%. Figure 23 illustrates the effect of the internal tube size on the time-averaged gas holdup at the operation condition of a superficial gas velocity of $U_g = 0.2$ m/s. As shown in Figure 23, the bubble column with 1 in. internals provides a higher gas holdup than the bubble column with 0.5 in. internals at the region between $r/R = 0.15-0.4$ and the region between $r/R = 0.6-0.8$.

In addition, the bubble column without vertical internal tubes exhibited the gas holdup radial profile in a smooth parabolic shape for all studied gas velocities. In contrast, the bubble columns equipped with dense vertical internal tubes displayed wavy-shaped profiles along with a parabolic trend for all

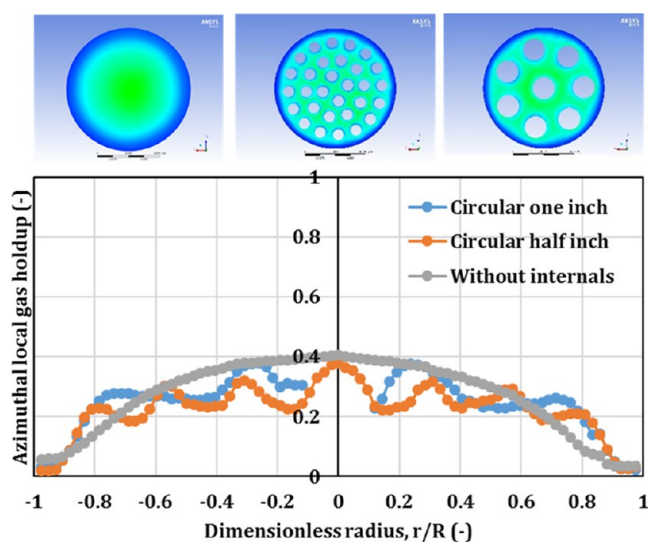


Figure 23. Effect of the internal tube size on the time-averaged gas holdup distribution and diameter profile at $U_g = 0.2$ m/s.

investigated configurations of the vertical internals. These wavy profiles for the bubble columns with vertical internal tubes varied according to the configurations of the vertical internals in the bubble column. The variation of gas holdup profiles in bubble columns with vertical internals was due to the different arrangements of the tubes over the cross-sectional area (CSA) of the column, the shape of the pitch for each configuration, and the space (clearance) between the bundle of vertical internals and the column wall. Each concave area of these profiles represents the azimuthal average of the gas holdup values in the spaces among the vertical internal tubes. These kinds of wavy gas holdup profiles have not been reported in the literature for a

bubble column with dense vertical internals when measured by optical probes.^{63,6} However, these wavy profiles have been reported by Al Mesfer et al.⁴¹ when they measured the gas holdup in the bubble column with dense vertical internals using the CT technique.

Figure 24 illustrates the two-dimensional (2D) images of the CFD time-averaged cross-sectional gas holdup in the bubble column without internals and in the bubble column equipped with a different configuration of internals (hexagonal and circular) and different internal tube diameters (0.5 and 1 in.). As can be seen, in the bubble column without internals, the higher magnitudes of gas holdup are in the core of the bubble column, while the lower gas holdup is in the wall region of the column. This phenomenon still exists in the presence of internals in different configurations and different internal tube diameters, as shown in Figure 24b–d. Further, a similar observation was indicated in Figure 19 in terms of various gas velocities, where the magnitudes of the gas holdup increased with the increase in the superficial gas velocities in bubble columns with and without internals. However, this phenomenon agrees with the results that have been reported by Sultan et al.⁶⁶ Based on their visualization that explains this phenomenon, the common core-annulus (ascending of liquid in the center and liquid descending on the wall region) liquid circulation is very similar to that obtained in the bubble column without internals.

5. REMARKS

3D time-dependent simulations of two-phase bubble columns using the commercial CFD code have been accomplished to validate the turbulent models (RNG ($k - \epsilon$) and standard ($k - \epsilon$)) and the interfacial forces (the drag force, lift force, wall lubrication force, and turbulent dispersion force). Furthermore, the effects of the presence of internals, the configurations of internals (hexagonal and circular arrangements), and the

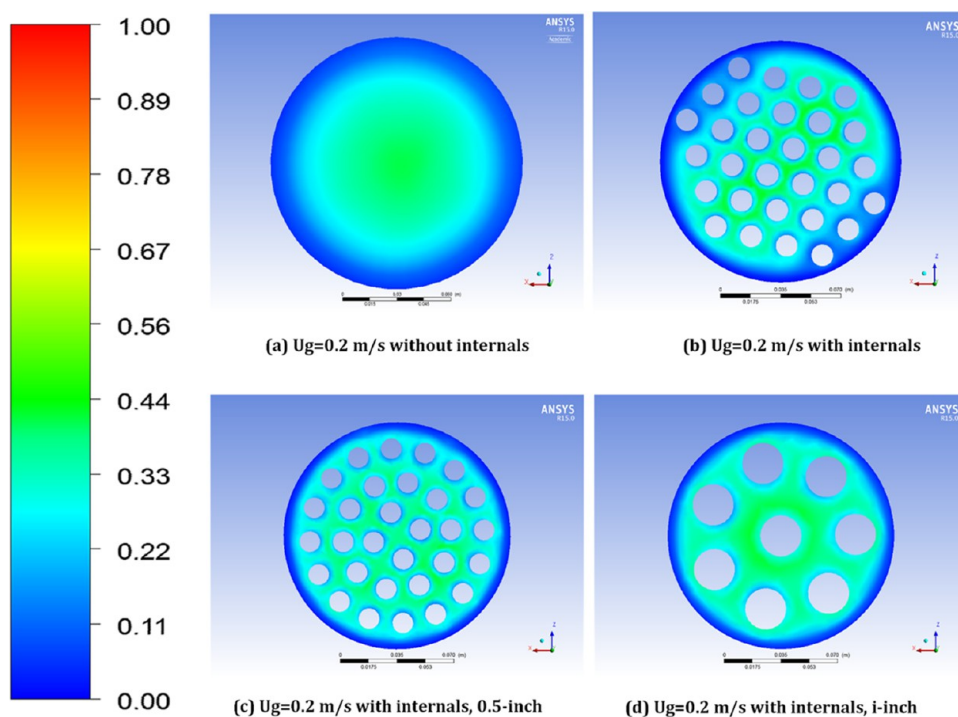


Figure 24. CFD simulations of the effect of the internal configurations and internal tube diameter on the time-averaged cross-sectional gas holdup distributions.

internals tube diameters on the time-averaged gas holdup distributions have been addressed. Accordingly, the current simulation results reveal the following remarks:

51. The validation results indicated the inability to use the drag force as a singular interfacial force to predict the hydrodynamics of the bubble column, while applying a combination of interfacial forces of the drag, lift, wall lubricating, and turbulent dispersion properly would significantly improve the simulation results in terms of the profile and the magnitude value of the gas holdup.
52. Interfacial force models including the drag force, the wall lubrication force, and the turbulent dispersion force that were proposed by Grace et al.,⁵¹ Antal et al.,⁵⁸ and Simonin and Viollet,⁶⁰ respectively, exhibit better prediction results, in terms of the average absolute relative difference (AARD) = 17% for the time average of the gas holdup distributions. Meanwhile, the prediction of liquid velocity using the turbulent model of RNG ($k - \epsilon$) shows a good agreement with the experimental results about (AARD) = 17.6%, in particular, in the central and the wall regions of the bubble column and the reflecting point that is located at $r/R \sim 0.69$, whereas the standard ($k - \epsilon$) model lost the prediction in these regions.
53. Incorporation of the population balance model (PBM), in turn, improves the performance of the numerical solution in a wide range of the used superficial gas velocity (the bubbly flow and the churn turbulent flow regimes). However, the simulation results of the time-averaged gas holdup distributions operated at a turbulent flow regime of $U_g = 0.2$ m/s illustrate a high sensitivity toward the variation in the numbers of bubble groups. Further, it has been revealed that the used classes of bubbles with 20 groups illustrate a good agreement for the simulation results with the experimental results about (AARD = 16.8%).
54. Validated CFD closures (i.e., interfacial forces and the turbulent model) exhibit the capability of predicting the hydrodynamics of the bubble column that are estimated based on comparison with the experimental results by the average absolute relative difference (AARD). In the case of the bubble column without internals, the average absolute relative difference is AARD= 14.6, 16.8, and 16.2% for gas velocities $U_g = 0.05, 0.2,$ and 0.45 m/s, respectively, while in the case of bubble column with internals, the average absolute relative differences are AARD = 29.5, 24.8, and 15.9% for gas velocities $U_g = 0.05, 0.2,$ and 0.45 m/s, respectively. Furthermore, the numerical solution appears to be capable of capturing the effect of the internal design variation that includes different configurations and different internal tube diameters on the gas holdup profiles. Hence, we expect that the numerical solution will provide the opportunity to understand the transport phenomena in bubble columns that operated in severe operating conditions (high temperature and pressure) in terms of the low cost of the experiment and the flexibility in designing.
55. In the bubble column with and without internals, the magnitude value of the time-averaged gas holdup was increased significantly with an increase in the superficial gas velocity, particularly in the central region of the column. Furthermore, the simulation results, obtained in a low superficial gas velocity of $U_g = 0.05$ m/s, appear that the gas holdup profiles over the cross section of the bubble column with and without internals have a semiflat shape. As the superficial gas velocity increases, the gas holdup profiles are steeper (i.e., increase the difference in the magnitude value of the gas holdup between the central and wall regions). This phenomenon leads to the fact that the increase in the superficial gas velocity will promote liquid circulation in the bubble column.
56. The 2D images of the CFD scan for the time-averaged cross-sectional gas holdup in the bubble column with and without internals reveal the core-annular liquid circulation pattern, which is commonly prevalent in the bubble column without internals, still existing in bubble column internals.
57. The simulation results exhibit no significant effect for the presence of internals (all used designed internals) on the time-averaged gas holdup distributions in the central region of the bubble column, whereas the presence of internals significantly increases the gas holdup close to the wall region of the bubble column.
58. At a high superficial gas velocity, the time-averaged gas holdup distributions over the cross section of the bubble column without internals appear in a smooth-line parabolic, whereas the gas holdup distributions exhibit wavy line profiles in the presence of internals (at all used designed internals). Therefore, the variation in the gas holdup profiles is related to the numbers of internal tubes, the gaps between the tubes, and the size of the internals.
59. The results of the effect of the internal diameter exhibit that the gas holdup was remarkably increased in the center and the wall regions of the bubble column equipped by internals of 1 in. diameter more than the other used designed internals. Meanwhile, the effect of internal configurations reported that the internals with a hexagonal arrangement increase the gas holdup in the central region more than the circular arrangement (of 0.5 in.) and less in the wall region compared with that in the circular arrangement. Accordingly, the time-averaged gas holdup distributions exhibit a significant alteration in terms of the profiles and the magnitude toward the variation in the internal configuration and internal tube diameters.

■ AUTHOR INFORMATION

Corresponding Author

Muthanna H. Al-Dahhan – Mining and Nuclear Engineering Department, Missouri University of Science and Technology, Rolla, Missouri 65409, United States; Chemical and Biochemical Engineering Department and Linda and Bipin Doshi Chemical and Biochemical Engineering Department, Missouri University of Science and Technology, Rolla, Missouri 65409, United States; TechCell, Mohammed VI Polytechnic University, 43150 Ben Guerir, Morocco; Email: aldahhan@mst.edu

Authors

Hayder Al-Nasari – Chemical Engineering Department, Tikrit University, Tikrit 34001, Iraq; orcid.org/0000-0001-6490-7179

J. P. Schlegel – Mining and Nuclear Engineering Department, Missouri University of Science and Technology, Rolla, Missouri 65409, United States

Complete contact information is available at:
<https://pubs.acs.org/10.1021/acs.iecr.3c01404>

Notes

This research is part of a thesis deposited as a Ph.D. thesis and the corresponding Digital Object Identifier (DOI: 10.1016/0300-9467(86)80035-1).

The authors declare no competing financial interest.

ACKNOWLEDGMENTS

The authors gratefully acknowledge financial support in the form of a scholarship provided by the Higher Committee for Education Development in Iraq (HCED) and the funds provided by Multiphase Flow Reactors Engineering and Applications Laboratory (mFReal) to develop the four-point optical fiber probe technique, as well as Phillips 66 for the experimental setup used to perform the present study.

REFERENCES

- (1) Wu, C.; Al-Dahhan, M. Heat Transfer Coefficients in Mimicked Fischer–Tropsch Slurry Bubble Columns. *Ind. Eng. Chem. Res.* **2012**, *51* (4), 1543–1548.
- (2) Barghi, S.; Prakash, A.; Margaritis, A.; Bergougnou, M. A. Flow Regime Identification in a Slurry Bubble Column from Gas Holdup and Pressure Fluctuations Analysis. *Can. J. Chem. Eng.* **2008**, *82* (October), 865–870.
- (3) Rzehak, R.; Krauß, M.; Kováts, P.; Zähringer, K. Fluid dynamics in a bubble column: New experiments and simulations. *Int. J. Multiphase Flow* **2017**, *89*, 299–312.
- (4) Rabha, S.; Schubert, M.; Hampel, U. Intrinsic flow behavior in a slurry bubble column: A study on the effect of particle size. *Chem. Eng. Sci.* **2013**, *93*, 401–411.
- (5) Sasaki, S.; Uchida, K.; Hayashi, K.; Tomiyama, A. Effects of column diameter and liquid height on gas holdup in air–water bubble columns. *Exp. Therm. Fluid Sci.* **2017**, *82*, 359–366.
- (6) Al-Naseri, H.; Schlegel, J. P.; Al-Dahhan, M. H. The effects of internals and low aspect ratio on the fully developed flow region and bubble properties in a pilot-plant bubble column. *Exp. Therm. Fluid Sci.* **2019**, *104* (October), 284–301.
- (7) Yang, G.; Guo, K.; Wang, T. Numerical simulation of the bubble column at elevated pressure with a CFD-PBM coupled model. *Chem. Eng. Sci.* **2017**, *170* (October), 251–262.
- (8) Basha, O. M.; Weng, L.; Men, Z.; Morsi, B. I. CFD Modeling with Experimental Validation of the Internal Hydrodynamics in a Pilot-Scale Slurry Bubble Column Reactor. *Int. J. Chem. React. Eng.* **2016**, *14* (2), 599–619.
- (9) Syed, A. H.; Boulet, M.; Melchiori, T.; Lavoie, J. M. CFD simulation of a slurry bubble column: Effect of population balance kernels. *Comput. Fluids* **2018**, *175*, 167–179.
- (10) Youssef, A. A.; Hamed, M. E.; Grimes, J. T.; Al-Dahhan, M. H.; Duduković, M. P. Hydrodynamics of pilot-scale bubble columns: Effect of internals. *Ind. Eng. Chem. Res.* **2013**, *52* (1), 43–55.
- (11) Youssef, A. A.; Al-Dahhan, M. H. Impact of internals on the gas holdup and bubble properties of a bubble column. *Ind. Eng. Chem. Res.* **2009**, *48* (17), 8007–8013.
- (12) Gemello, L.; Plais, C.; Augier, F.; Cloupet, A.; Marchisio, D. L. Hydrodynamics and bubble size in bubble columns: Effects of contaminants and spargers. *Chem. Eng. Sci.* **2018**, *184*, 93–102.
- (13) Thorat, B. N. N.; et al. Effect of Sparger Design and Height to Diameter Ratio on Fractional Gas Hold-up in Bubble Columns. *Chem. Eng. Res. Des.* **1998**, *76* (7), 823–834.
- (14) Doshi, Y. K.; Pandit, A. B. Effect of internals and sparger design on mixing behavior in sectionalized bubble column. *Chem. Eng. J.* **2005**, *112* (1–3), 117–129.
- (15) Wu, C.; Al-Dahhan, M. H.; Prakash, A. Heat transfer coefficients in a high-pressure bubble column. *Chem. Eng. Sci.* **2007**, *62* (1–2), 140–147.
- (16) Guan, X.; Li, Z.; Wang, L.; Cheng, Y.; Li, X. CFD simulation of bubble dynamics in bubble columns with internals. *Ind. Eng. Chem. Res.* **2014**, *53* (42), 16529–16538. 2014
- (17) Das, A. K.; Das, P. K.; Thome, J. R. Transition of Bubbly Flow in Vertical Tubes: New Criteria Through CFD Simulation. *J. Fluids Eng.* **2009**, *131* (9), 091304.
- (18) van Baten, J. M.; Krishna, R. CFD Simulations of a Bubble Column Operating in the Homogeneous and Heterogeneous Flow Regimes. *Chem. Eng. Technol.* **2002**, *25* (11), 1081–1086.
- (19) Troshko, A. A.; Zdravistich, F. CFD modeling of slurry bubble column reactors for Fischer–Tropsch synthesis. *Chem. Eng. Sci.* **2009**, *64* (5), 892–903.
- (20) Gemello, L.; Cappello, V.; Augier, F.; Marchisio, D.; Plais, C. CFD-based scale-up of hydrodynamics and mixing in bubble columns. *Chem. Eng. Res. Des.* **2018**, *136* (69), 846–858.
- (21) Bhusare, V. H.; Dhiman, M.; Kalaga, D.; et al. CFD simulations of a bubble column with and without internals by using OpenFOAM. *Chem. Eng. J.* **2017**, *317*, 157–174.
- (22) Dhotre, M. T.; Ekambara, K.; Joshi, J. B. CFD simulation of sparger design and height to diameter ratio on gas hold-up profiles in bubble column reactors. *Exp. Therm. Fluid Sci.* **2004**, *28* (5), 407–421.
- (23) Ekambara, K.; Dhotre, M. T.; Joshi, J. B. CFD simulations of bubble column reactors: 1D, 2D and 3D approach. *Chem. Eng. Sci.* **2005**, *60* (23), 6733–6746.
- (24) An, M.; Guan, X.; Yang, N.; Bu, Y.; Xu, M.; Men, Z. Effects of internals on fluid dynamics and reactions in pilot-scale slurry bubble column reactors: A CFD study for Fischer–Tropsch synthesis. *Chem. Eng. Process.: Process Intensif.* **2018**, *132* (August), 194–207.
- (25) Law, D.; Battaglia, F.; Heindel, T. Stability issues for gas–liquid flows in bubble columns. In *Volume 8: Heat Transfer, Fluid Flows, and Thermal Systems, Parts A and B*, ASME International Mechanical Engineering Congress and Exposition, ASME, 2007; pp 53–61. DOI: 10.1115/IMECE2007-43517.
- (26) Delnoij, E.; Lammers, F. A.; Kuipers, J. A. M.; Van Swaaij, W. P. M. Dynamic simulation of dispersed gas–liquid two-phase flow using a discrete bubble model. *Chem. Eng. Sci.* **1997**, *52* (9), 1429–1458.
- (27) Delnoij, E.; Kuipers, J. A. M.; van Swaaij, W. P. M. Dynamic simulation of gas–liquid two-phase flow: effect of column aspect ratio on the flow structure. *Chem. Eng. Sci.* **1997**, *52* (21–22), 3759–3772.
- (28) Delnoij, E.; Kuipers, J. A. M.; Van Swaaij, W. P. M. Computational fluid dynamics applied to gas–liquid contactors. *Chem. Eng. Sci.* **1997**, *52*, 3623.
- (29) Rampure, M. R. Modelling of Gas–liquid/Gas–liquid–solid Flows in Bubble Columns: Experiments and CFD Simulations. *Can. J. Chem. Eng.* **2008**, *81* (3–4), 692–706.
- (30) Sanyal, J.; Vásquez, S.; Roy, S.; Dudukovic, M. P. Numerical simulation of gas–liquid dynamics in cylindrical bubble column reactors. *Chem. Eng. Sci.* **1999**, *54* (21), 5071–5083.
- (31) Sokolichin, A.; Eigenberger, G. Gas–liquid flow in bubble columns and loop reactors: Part I. Detailed modelling and numerical simulation. *Chem. Eng. Sci.* **1994**, *49* (24), 5735–5746.
- (32) Pan, Y.; Dudukovic, M. P.; Chang, M. Numerical investigation of gas–driven flow in 2-D bubble columns. *AIChE J.* **2000**, *46* (3), 434–449.
- (33) Monahan, S. M.; Vitankar, V. S.; Fox, R. O. CFD predictions for flow-regime transitions in bubble columns. *AIChE J.* **2005**, *51* (7), 1897–1923.
- (34) Larachi, F.; Desvigne, D.; Donnat, L.; Schweich, D. Simulating the effects of liquid circulation in bubble columns with internals. *Chem. Eng. Sci.* **2006**, *61* (13), 4195–4206.
- (35) Guo, X.; Chen, C. Simulating the impacts of internals on gas–liquid hydrodynamics of bubble column. *Chem. Eng. Sci.* **2017**, *174*, 311–325.
- (36) Kagumba, M.; Al-Dahhan, M. H. Impact of Internals Size and Configuration on Bubble Dynamics in Bubble Columns for Alternative Clean Fuels Production. *Ind. Eng. Chem. Res.* **2015**, *54* (4), 1359–1372.
- (37) Guan, X.; Yang, N. CFD simulation of pilot-scale bubble columns with internals: Influence of interfacial forces. *Chem. Eng. Res. Des.* **2017**, *126*, 109–122.

- (38) Yu, Z.; Jia, L.; Lijun, W.; Xi, L. Studies on hydrodynamics of turbulent slurry bubble column(III) Effect of vertical pipe bundles. *J. Chem. Ind. Eng. Soc. China* **2009**, *60*, 1135–1140.
- (39) Agahzamin, S.; Pakzad, L. A comprehensive CFD study on the effect of dense vertical internals on the hydrodynamics and population balance model in bubble columns. *Chem. Eng. Sci.* **2019**, *193*, 421–435.
- (40) Youssef, A. *Fluid Dynamics and Scale-up of Bubble Columns with Internals*; Washington University in St. Louis, 2010. DOI: 10.1017/CBO9781107415324.004.
- (41) Al Mesfer, M. K.; Sultan, A. J.; Al-Dahhan, M. H. Impacts of dense heat exchanging internals on gas holdup cross-sectional distributions and profiles of bubble column using gamma ray Computed Tomography (CT) for FT synthesis. *Chem. Eng. J.* **2016**, *300*, 317–333.
- (42) Drew, D. A.; Lahey, R. T., Jr Application of General Constitutive Principles To the Derivation of Multidimensional Two-Phase Flow Equations. *Int. J. Multiphase Flow* **1979**, *5* (4), 243–264.
- (43) Sato, Y.; sadatomi, M.; Sekoguchi, K. Momentum and heat transfer in two-phase bubble flow-I. *Int. J. Multiphase Flow* **1981**, *7*, 167–177.
- (44) Pourtousi, M.; Ganesan, P.; Sahu, J. N. Effect of bubble diameter size on prediction of flow pattern in Euler-Euler simulation of homogeneous bubble column regime. *Measurement* **2015**, *76*, 255–270.
- (45) Pourtousi, M.; Sahu, J. N.; Ganesan, P.; Shamshirband, S.; Redzwan, G. A combination of computational fluid dynamics (CFD) and adaptive neuro-fuzzy system (ANFIS) for prediction of the bubble column hydrodynamics. *Powder Technol.* **2015**, *274*, 466–481.
- (46) Behzadi, A.; Issa, R. I.; Rusche, H. Modelling of dispersed bubble and droplet flow at high phase fractions. *Chem. Eng. Sci.* **2004**, *59* (4), 759–770.
- (47) Azimi Yancheshme, A.; Zarkesh, J.; Rashtchian, D.; Anvari, A. CFD Simulation of Hydrodynamic of a Bubble Column Reactor Operating in Churn-Turbulent Regime and Effect of Gas Inlet Distribution on System Characteristics. *Int. J. Chem. React. Eng.* **2016**, *14* (1), 213–224.
- (48) Zhu, Z.; Cao, G.; Wu, R. Computational Fluid Dynamics Modeling of Rope-Guided Conveyances in Two Typical Kinds of Shaft Layouts. *PLoS One* **2015**, *10* (2), No. e0118268.
- (49) Yeoh, G. H.; Tu, J. *Computational techniques for Multi-Phase Flows*; Elsevier Ltd: UK, 2010.
- (50) Li, G.; Yang, X.; Dai, G. CFD simulation of effects of the configuration of gas distributors on gas-liquid flow and mixing in a bubble column. *Chem. Eng. Sci.* **2009**, *64* (24), 5104–5116.
- (51) Grace, J. R.; Wairegi, T.; Nguyen, T. H. Shapes and Velocities of Single Drops and Bubbles Moving Freely through Immiscible Liquids. *Trans. Inst. Chem. Eng.* **1976**, *54* (3), 167–173.
- (52) Tomiyama, A. Struggle with computational bubble dynamics. *Multiphase Sci. Technol.* **1998**, *10* (4), 369–405.
- (53) Morsi, S. A.; Alexander, A. J. An investigation of particle trajectories in two-phase flow systems. *J. Fluid Mech.* **1972**, *55* (2), 193–208.
- (54) Schiller, L.; Naumann, Z.; Deutscher, L. A Drag Coefficient Correlation. *VDI Zeitung* **1935**, *77* (0341–7255), 318–320.
- (55) Bothe, D.; Schmidtke, M.; Warnecke, H. J. VOF-simulation of the lift force for single bubbles in a simple shear flow. *Chem. Eng. Technol.* **2006**, *29* (9), 1048–1053.
- (56) Lucas, D.; Krepper, E.; Prasser, H. M. Use of models for lift, wall and turbulent dispersion forces acting on bubbles for poly-disperse flows. *Chem. Eng. Sci.* **2007**, *62* (15), 4146–4157.
- (57) Yeoh, G. H.; Cheung, C. P.; Tu, J. *Multiphase Flow Analysis Using Population Balance Modeling*; Elsevier Ltd., 2014.
- (58) Antal, S. P.; Jr, R. T. L.; Flaherty, J. E. Analysis of Phase Distribution in Fully Developed Laminar Bubbly Two-Phase Flow. *Int. J. Multiphase Flow* **1991**, *17* (5), 635–652.
- (59) Frank, T.; Shi, J. M.; Burns, A. D. Validation of Eulerian multiphase flow models for nuclear safety application. In *3rd Int. Symp. Two-Phase Flow Model. Exp. Pisa 22–24 Sept. 2004*, no. September, pp 22–24. DOI: 10.1364/OE.26.001825.
- (60) Simonin, O.; Viollet, P. Modelling of turbulent two-phase jets loaded with discrete particles. *Phenom. Multiphase Flows* **1990**, 259–269.
- (61) Burns, A. D.; Frank, T.; Hamill, I.; Shi, J.-M. M. The Favre Averaged Drag Model for Turbulent Dispersion in Eulerian Multi-Phase Flows. In *Fifth Int. Conf. Multiph. Flow May 30-Jun 04 2004, Okohama, Japan*, p 392. http://www.drthfrank.de/publications/2004/Burns_Frank_ICMF_2004_final.pdf.
- (62) Kagumba, M.; Al-Naseri, H.; Al-Dahhan, M. H. A new contact time model for the mechanistic assessment of local heat transfer coefficients in bubble column using both the four-optical fiber probe and the fast heat transfer probe-simultaneously. *Chem. Eng. J.* **2019**, *361*, 67–79.
- (63) Luo, H.; Svendsen, H. F. Theoretical model for drop and bubble breakup in turbulent dispersions. *AIChE J.* **1996**, *42* (5), 1225–1233.
- (64) Luo, H. Coalescence, Breakup and Liquid Circulation in Bubble Column Reactors. the Institute of Norwegian Institute; The University of Trondheim: Trondheim, Norway, 1993.
- (65) Liang, X.-F.; Pan, H.; Su, Y.; Luo, Z. CFD-PBM approach with modified drag model for the gas-liquid flow in a bubble column. *Chem. Eng. Res. Des.* **2016**, *112*, 88–102.
- (66) Sultan, A. J.; Sabri, L. S.; Al-Dahhan, M. H. Influence of the size of heat exchanging internals on the gas holdup distribution in a bubble column using gamma-ray computed tomography. *Chem. Eng. Sci.* **2018**, *186*, 1–25.
- (67) Sultan, A. J.; Sabri, L. S.; Al-Dahhan, M. H. Impact of heat-exchanging tube configurations on the gas holdup distribution in bubble columns using gamma-ray computed tomography. *Int. J. Multiphase Flow* **2018**, *106*, 202–219.
- (68) Sultan, A. J.; Sabri, L. S.; Al-Dahhan, M. H. Investigating the influence of the configuration of the bundle of heat exchanging tubes and column size on the gas holdup distributions in bubble columns via gamma-ray computed tomography. *Exp. Therm. Fluid Sci.* **2018**, *98* (February), 68–85.
- (69) Sultan, A. J.; Sabri, L. S.; Shao, J.; Al-Dahhan, M. H. Overcoming the gamma-ray computed tomography data processing pitfalls for bubble column equipped with vertical internal tubes. *Can. J. Chem. Eng.* **2018**, *96*, 2206–2226.
- (70) Krishna, R.; Ellenberger, J.; Hennophof, D. E. Analogous description of the hydrodynamics of gas-solid fluidized beds and bubble columns. *Chem. Eng. J. Biochem. Eng. J.* **1993**, *53* (1), 89–101.
- (71) Ellenberger, J.; Krishna, R. A unified approach to the scale-up of gas-solid fluidized bed and gas-liquid bubble column reactors. *Chem. Eng. Sci.* **1994**, *49* (24), 5391–5411.
- (72) Wu, Y.; Al-Dahhan, M. H. Prediction of axial liquid velocity profile in bubble columns. *Chem. Eng. Sci.* **2001**, *56* (3), 1127–1130.
- (73) Mutharasu, L. C.; Kalaga, D. V.; Sathe, M.; Turney, D. E.; Griff, D.; Xueliang, L.; Kawaji, M.; Nandakumar, M.; Joshi, J. B. Experimental study and CFD simulation of the multiphase flow conditions encountered in a Novel Down-flow Bubble Column. *Chem. Eng. J.* **2018**, *350* (April), 507–522.
- (74) Silva, M. K.; Akira d'Ávila, M.; Mori, M. Study of the interfacial forces and turbulence models in a bubble column. *Comput. Chem. Eng.* **2012**, *44*, 34–44.
- (75) Tabib, M. V.; Roy, S. A.; Joshi, J. B. CFD simulation of bubble column — An analysis of interphase forces and turbulence models. *Chem. Eng. J.* **2008**, *139*, 589–614.
- (76) Yamoah, S.; Martínez-Cuenca, R.; Monrós, G.; Chiva, V.; Macián-Juan, R. Numerical investigation of models for drag, lift, wall lubrication and turbulent dispersion forces for the simulation of gas-liquid two-phase flow. *Chem. Eng. Res. Des.* **2015**, *98*, 17–35.
- (77) Chen, P.; Sanyal, J.; Dudukovic, M. P. CFD modeling of bubble columns flows: Implementation of population balance. *Chem. Eng. Sci.* **2004**, *59* (22–23), 5201–5207.
- (78) Al Mesfer, M. K.; Sultan, A. J.; Al-Dahhan, M. H. Study the Effect of Dense Internals on the Liquid Velocity Field and Turbulent Parameters in Bubble Column for Fischer–Tropsch (FT) Synthesis by Using Radioactive Particle Tracking (RPT) Technique. *Chem. Eng. Sci.* **2017**, *161*, 228–248.

(79) Versteeg, H. K.; Malalasekera, W. *An Introduction to Computational Fluid Dynamics: The finite volume method*; Pearson Education Limited: UK, 2007.

(80) Kumar, S. B. Computed Tomographic Measurements of Void Fraction and Modeling of the Flow in Bubble Columns. Ph.D. Thesis. Washington University: St. Louis, MO, 1994.

(81) Rados, N.; Shaikh, A.; Al-Dahhan, M. H. Solids flow mapping in a high pressure slurry bubble column. *Chem. Eng. Sci.* **2005**, *60* (22), 6067–6072.

(82) Nedeltchev, S.; Shaikh, A. A new method for identification of the main transition velocities in multiphase reactors based on information entropy theory. *Chem. Eng. Sci.* **2013**, *100*, 2–14.

(83) Chen, J.; Fan, L.; Degaleesan, S.; Gupta, P.; Al-Dahhan, M. H.; Duduković, M. P.; Toseland, B. A. Fluid dynamic parameters in bubble columns with internals. *Chem. Eng. Sci.* **1999**, *54* (13–14), 2187–2197.